공학박사학위논문

Synthesis and Characterization of Photo/thermo Cross-linkable Self-healing Polymers and Fluorine-functionalized Graphene Oxide/Nafion Composite Membrane for Redox Flow Battery

광/열가교성 자가치유 고분자 및 레독스 흐름 전지용 불소-기능화된 그래핀옥사이드/나피온 복합체막의 합성과 분석

2017년 2월

서울대학교 대학원

화학생물공학부

최 원 재

Synthesis and Characterization of Photo/thermo Cross-linkable Self-healing Polymers and Fluorine-functionalized Graphene Oxide/Nafion Composite Membrane for Redox Flow Battery

by

Won Jae Choi

Adviser: Professor Jong-Chan Lee, Ph. D.

Submitted in Partial Fulfillment
of the Requirements for the Degree of
DOCTOR OF PHILOSOPHY

February, 2017

School of Chemical and Biological Engineering
College of Engineering
Graduate School
Seoul National University

Abstract

Synthesis and Characterization of Photo/thermo Cross-linkable Self-healing Polymers and Fluorine-functionalized Graphene Oxide/Nafion Composite Membrane for Redox Flow Battery

Won Jae Choi

Chemical and Biological Engineering, Polymer Chemistry

The Graduate School

Seoul National University

In this report, synthesis and characterization of photo/thermo cross-linkable self-healing polymers and fluorine-functionalized graphene oxide/Nafion composite membrane for redox flow battery. Firstly, methacrylate derivative having photo cross-linkable cinnamate functional group (PCEMA) was synthesized via free radical polymerization. The reversible cross-linking reaction of functional group of PCEMA by changing the wavelength of irradiated UV was confirmed. And the

self-healing property at over its glass transition temperature was investigated by monitoring the self-healing property of synthesized methacrylate derivatives with similar structure and different glass transition temperature. Synthesized polymers showed self-healing property over its glass transition temperature by chain entanglement without any chemical reaction. Through this, self-healing polymer with surface hardness control was synthesized and characterized successfully.

Secondly, methacrylate derivatives with thermally cross-linkable furan functionality were synthesized by free radical polymerization. And the self-healing polymeric system with enhanced mechanical property was prepared using Diels-Alder reaction with synthesized polymers and maleimide cross-linker. The reactivity of Diels-Alder reaction of furan functionality of polymers were intentionally varied with electron density to investigate its influence to the self-healing property. By increasing the electron density of furan functionality, Diels-Alder reaction with maleimide cross-linker was increased. Through this, it is confirmed that the self-healing property was affected by the reactivity of the healing-inducing functionality.

Finally, fluoroalkyl-functionalized graphene oxide (FGO)/Nafion composite membrane was prepared to enhance the performance of Nafion membrane in redox flow battery application. Although composite membrane showed low water uptake and proton conductivity due to the hydrophobicity of introduced fluorine,

its dimensional stability was increased and vanadium ion permeability was decreased due to GO. Also, the overall RFB cell performance was increased result from the narrow and fine hydrophilic channel formation of membrane due to the enhanced compatibility with filler and Nafion.

Keyword: self-healing polymer, reversible covalent bond, redox flow battery, graphene oxide derivative, composite membrane.

Student Number: 2011-21082

TABLE OF CONTENT

Chapter 1

Introduction

Chapter 2

Healable Properties of Polymethacrylate Derivatives Having Photo Crosslinkable Cinnamoyl Side Groups with Surface Hardness Control

Chapter 3

The Study of Self-healing Property Change of Diels-Alder Based Polymeric Materials Affected by Reactivity of Furan Functionalities

Chapter 4

Fluoroalkyl-functionalized Graphene Oxide/Nafion Composite Membrane for All-Vanadium Redox Flow Battery

List of Figures

List of Tables

Chapter 1

Introduction

1.1. Self-healing polymers

Traditional polymeric material used in industry is usually faced with continuous fatigue, which can result in the impediment of performance or increment of repair/replace cost. Thus the self-healing materials have drawn tremendous of interests throughout the industry due to its characteristic ability to recover the macro/microscale of physical/chemical damage, leads to increased stability of whole system and cost efficiency.

There are two aspects to obtain this self-healing property to polymeric materials, interaction to recover the pristine property and mobility to fill the fracture void. After the damage, polymer chain can be diffused through the damaged area by its segmental mobility to draw reactive sites close. And chemical /physical interaction can be reformed as depicted in figure 1.1 [1]. There has been various studies up to date to meet these aforementioned prerequisites, and categorized to three different strategies.

One strategy is to embed healing agent into polymer matrix by using capsule or vascular model [2-4]. This was first developed by White et al by encapsulate dicyclopentadiene healing agent into epoxy resin which having dispersed Grubb's catalyst (Figure 1.2). In the case of this, catalyst should be dispersed in polymer matrix, stability and cost issues are to the fore. Furthermore, repeated healing of damage of identical area is hard to be obtained.

Other strategy is using supramolecular interaction to drive healing ability [5-6]. There have been many researches using ionomer, π-π stacking or hydrogen bonding formation. Leibler et al reported self-healing oligomeric material using hydrogen bond between di/triacid monomers and urea-functionalized oligomers. Figure 1.3 shows the chemical structure and schematic model of self-healing of copolymer containing multivalent hydrogen bonding sites reported by Campo et al [6]. Polymeric materials using this strategy have been vigorously studied due to its high repeatable healing efficiency despite of its relatively low mechanical properties.

Finally there are studies involves intrinsic reversible covalent bond formation such as Diels-Alder, photoreversible cycloaddition reactions, or radical formations [7-11]. This strategy has drawn many interests due to its reversible nature and feasibility to design polymers with high mechanical properties enough to be applied in industrial applications.

1.2. Ion exchange membranes for redox flow battery

Redox flow battery

There has been increasing demand for sustainable and renewable energy as solar, wind or geothermal due to depletion of fossil fuels and environmental issues. Although these energy sources can supply abundant amount of energy enough to replace fossil fuels, issues like its mismatch between power generation and consumption and unreliability due to environmental conditions such as weather should be controlled. Therefore it became important to develop an energy storage system to overcome aforementioned limitations of renewable energy sources. Among the various of energy storage systems such as secondary batteries and supercapacitors, redox flow battery (RFB) has been on the rise.

RFB was invented by the National Aeronautics and Space Administration (NASA) in the 1970s. This battery system contains two separated electrolytes and its external reservoirs and pumps, energy converting system comprised of stacked cells and energy consuming/generating source as depicted in figure 1.4 [12]. The key component that separates RFB from other energy storage system is the electrolytes containing redox pairs that can flow through energy converting system from external reservoir, which gives scalability and design-flexibility to

RFB system.

Since Taller introduced the first RFB model using ferric/ferrous halide and chromic/chromous halide solution as a positive and negative electrolyte, many types of RFBs using different redox pairs have been researched [13-14]. Among them, vanadium redox flow battery (VRFB) has been studied intensively due to utilization of same vanadium element with different oxidative states from V^{2+} to V^{5+} on both electrolytes so that the cross-contamination of electrolytes driven by ion diffusion can be minimized, apart from its fast response time and long lifespan.

Ion exchange membrane

Ion exchange membrane (IEM) is a key component in RFB system, which separates negative and positive electrolytes (anolyte and catholyte) and allows charge carriers such as protons or sulfate ions to permeate while prevents crossover of reactive species act as redox couple. IEM should meet some following requirements, high chemical and physical stability, high ionic conductivity and selectivity to maintain the RFB performance during long-term operation.

Nafion, a representative perfluorinated polymer membrane invented by DuPont, has been exclusively used due to its exceptional chemical stability which enough to stand the harsh acidic environment of RFB system and high ionic conductivity. However, there also have been many researches to replace Nafion membrane because of its low ion selectivity due to the large ion conducting channel size and high cost.

1.3. Motivation

Cross-linkable self-healing polymer

Among the aforementioned strategies, covalent bond formation was selected to further study due to its reversibility and feasibility of design. Wool et al. reported crack healing of polystyrene glasses and provided a microscopic theory around glass transition temperature [15-16]. In these studies, healable polymers require not only the mobility for healing but also the sufficient mechanical properties to be used in application fields. So it is very important issue to develop self-healing polymeric material with both high healing efficiency and mechanical properties. For this reason, in chapter 2 and 3, synthesis and characterization of cross-linkable self-healing polymeric materials using reversible covalent bond formation were studied.

Firstly we synthesized and prepared a coating material of photo cross-linkable methacrylate derivatives having cinnamoyl moiety in its chain end which can be reversibly cross-linked by UV irradiation. Chung et al. reported crack healing of cinnamate by photochemical [2+2] cycloaddition reaction and this was used to enhance the surface hardness of prepared polymer film [10]. Afterwards, self-healing ability induced by chain mobility and entanglement was investigated.

Secondly we synthesized a series of Diels-Alder based methacrylate copolymers to investigate the change of self-healing properties by introducing furan functionality with different electron density. There has been many researches of Diels-Alder based self-healing polymers, but there are no reports about the influence of the reactivity of Diels-Alder reaction on healing efficiency [17-20]. We studied broadly about both two aspects of self-healing, mobility and reaction, by designing and characterizing various polymers through chapter 2 and 3.

Ion exchange membranes for RFB

One typical strategy to improve IEMs, is enhance or supplement of conventional IEM, Nafion, by introducing fillers or composite membrane. Fillers such as modified silicate and graphene oxide (GO) were studied and characterized for enhancing chemical/physical properties of Nafion and increasing electrical efficiencies by reducing the permeability of reactive species [21-22]. Especially for GOs, the permeability of vanadium ions were greatly decreased with small amount of filler due to the barrier effect of GO, thus induced improved cell cycle performance. In chapter 4, GO was functionalized with perfluoroalkyl chain to enhance the compatibility and electrical properties of Nafion/modified GO composite membrane.

1.4. References

[1] Y. Yang, M. W. Urban, Chem. Soc. Rev., 2013. 42, 7446.

[2] S. R. White, N. R. Sottos, P. H. Geubelle, J. S. Moore, M. R. Kessler, S. R. Siram, E. N. Brown, and S. Viswanathan, Nature, 2001, 409, 794.

[3] S. H. Cho, H. M. Andersson, S. R. White, N. R. Sottos, and P. V. Braun, Adv. Mater., 2006, 18, 997.

[4] K. S. Toohey, N. R. Sottos, J. A. Lewis, J. S. Moore, and S. R. White, Nat. Mater., 2007, 6, 581.

[5] P. Cordier, F. Tournilhac, C. Soulie-Ziakovic, and L. Leibler, Nature, 2008, 451, 977.

[6] J. Cui and A. del Campo, Chem. Commun., 2012, 48, 9302.

[7] X. Chen, M. A. Dam, K. Ono, A. Mal, H. Shen, S. R. Nutt, K. Sheran, and F. Wudl, Science, 2002, 295, 1698.

[8] A. A. Kavitha and N. K. Singha, ACS Appl. Mater. Interfaces, 2009, 7, 1427.

[9] H. M. Klukovich, Z. S. Kean, S. T. Iacono, and S. L. Craig, J. Am. Chem. Soc., 2011, 133, 17882.

[10] C. M. Chung, Y. S. Roh, S. Y. Cho, and J. G. Kim, Chem. Mater., 2004, 16, 3982.

[11] J. A. Yoon, J. Kamada, K. Koynov, J. Mohin, R. Nicolay, Y. Zhang, A. C. Balazs, T. Kowalewski, and K. Matyjaszewski, Macromolecules, 2012, 45, 142.

[12] A. Z. Weber, M. M. Mench, J. P. Meyers, P. N. Ross, J. T. Gostick, Q. H. Liu, J. Appl. Electrochem., 2011, 41, 1137.

[13] L. H. Taller, The 9th Intersociety Energy Conversion Engineering Conference Proceedings, 1974, 924.

[14] L. H. Taller, US3996064, 1976.

[15] O. J. Mcgarel, R. P. Wool, J. Polym. Sci. Polym. Phys., 1987, 25, 2541.

[16] Y. H. Kim, R. P. Wool, Macromolecules, 1983, 16, 1115.

[17] G. Zhang, Q. Zhao, L. Yang, W. Zou, X. Xi, and T. Xie, ACS Macro Lett., 2016, 5, 805.

[18] G. B. Lyon, A. Baranek, and C. N. Bowman, Adv. Funct. Mater., 2016, 26, 1477.

[19] Z. Gou, Y. Zuo, and S. Feng, RSC Adv., 2016, 6, 73140.

[20] A. A. Kavitha and N. K. Singha, Macromolecules, 2010, 43, 3193.

[21] P. Trogadas, E. Pinot, T. F. Fuller, Electrochem., Solid-State Lett., 2012, 15, A5.

[22] L. Yu, F. Lin, L. Xu, J. Xi, RSC Adv., 2016, 6, 3756.

[23] D. Chen, S. Wang, M. Xiao, Y. Meng, Energy Environ. Sci. 2010, 3, 622.

[24] D. Chen, S. Wang, M. Xiao, Y. Meng, J. Power. Sources, 2010, 195, 2089.

[25] D. Chen, S. Wang, M. Xiao, Y. Meng, Energy Convers. Manage, 2010, 51, 2816.

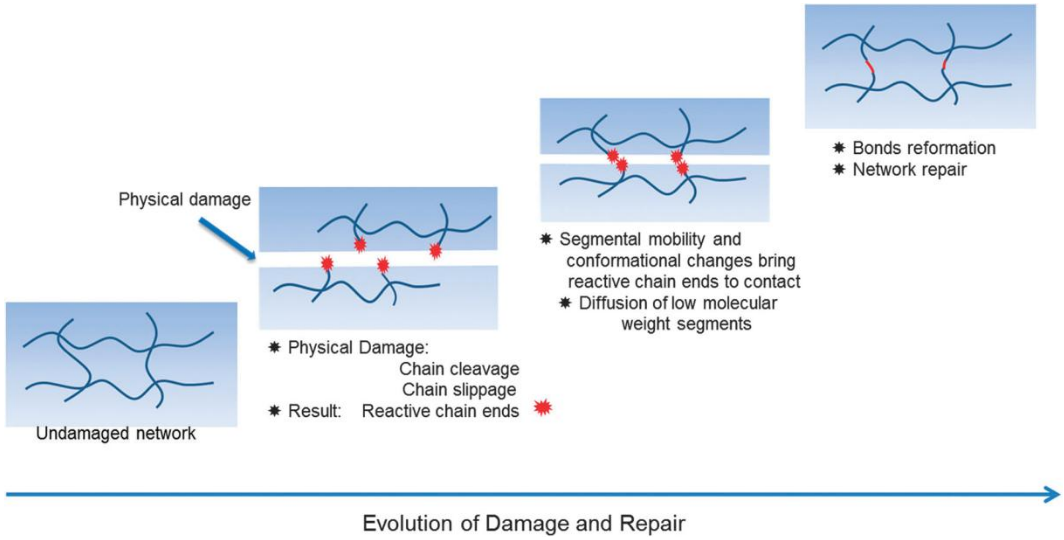

Figure 1.1. Schematic diagram of evolution of damage and repair of polymeric material [1].

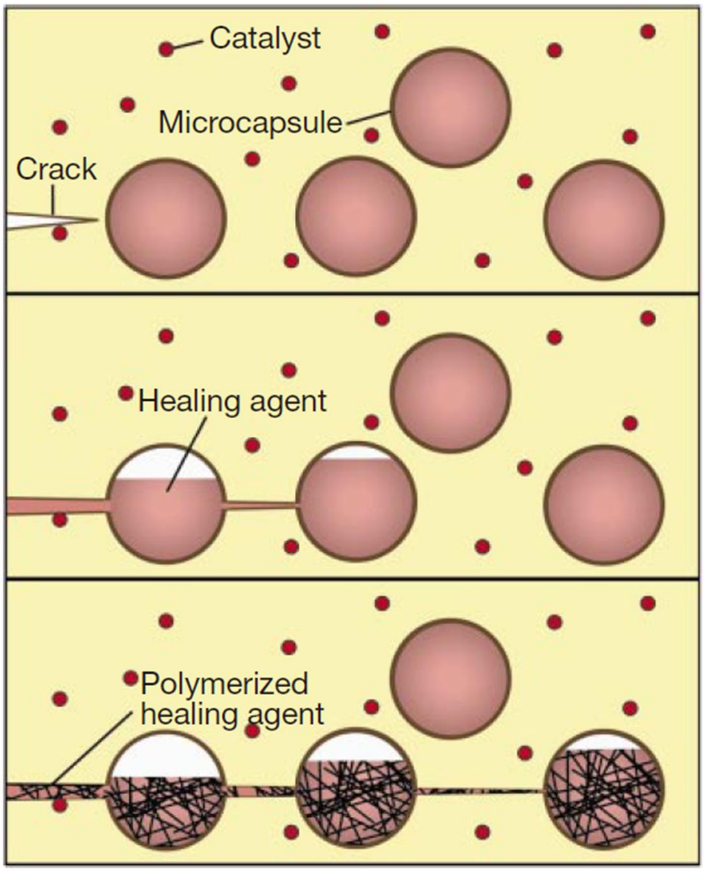

Figure 1.2. Schematic diagram of crack healing mechanism of encapsulated healing agent [2].

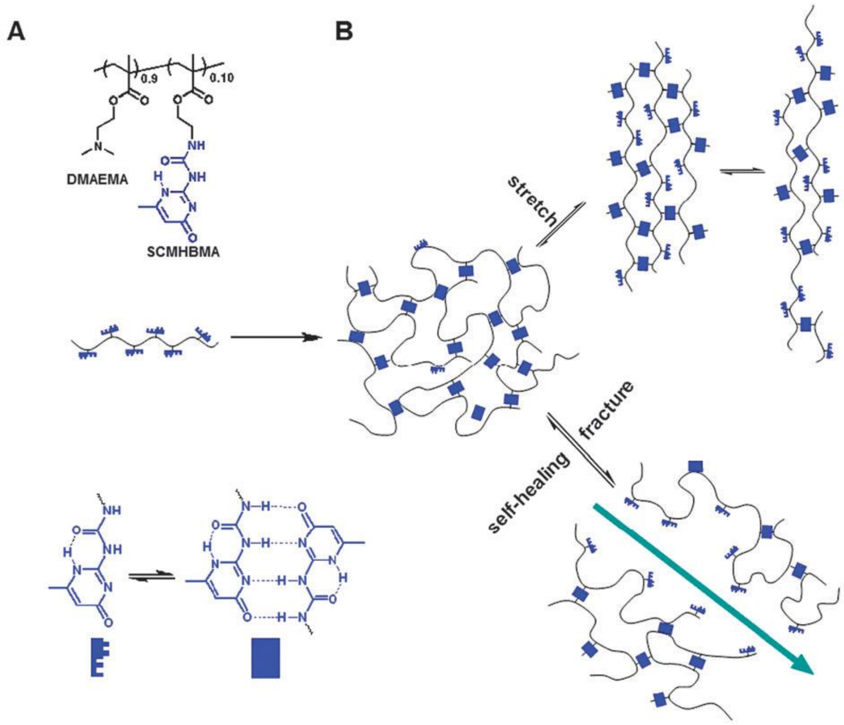

Figure 1.3. Chemical structure and schematic diagram of healing of multivalent hydrogen bond containing copolymer [6].

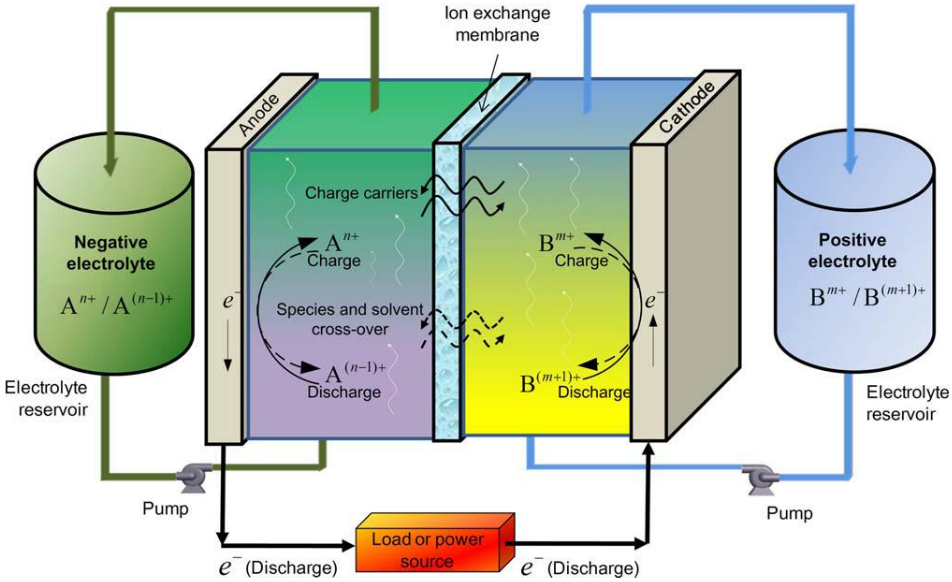

Figure 1.4. Schematic image of a RFB system [12].

Chapter 2

Healable Properties of Polymethacrylate Derivatives Having Photo Crosslinkable Cinnamoyl Side Groups with Surface Hardness Control

2.1. Introduction

There has been a growing interest in the study of the healable polymers due to the wide potential applications in electronics, the automotive industry, coatings, and so forth [1-3]. A major driving force for polymers as healable materials is the inter-diffusion of polymer chains into cracks above glass transition temperatures (T_g), where the chain mobility is high. Wool et al. reported craze healing in atatic polystyrene glasses and provided a microscopic theory around T_g for healing polymer and polymer/polymer interfaces [4,5]. Boiko et al. reported on the healing of a polymer/polymer interface around T_g [6]. While these studies present the possibility of polymers as healable materials, they require not only the mobility at the cracked area for healing but also the sufficient mechanical properties to use in various application fields. Therefore, the quest for efficient healable polymers with good mechanical properties remains as a great challenge. In this regard, there are two approaches to enhance the mechanical properties of healable polymers. The first involves intrinsic reversible crosslinking reaction in the polymer matrix such as Diels–Alder [7–9] or cycloaddition reactions [10,11]. The chemical structures of healed polymers are identical to that of the original ones via the reversible reactions, which in turn preserves the mechanical properties in the polymer matrix after the healing processes. The second involves the extrinsic addition of healing agents that can polymerize in the polymer matrix. The healing agents are released when cracks are generated, and then polymerizations of the healing agents inside the crack with the help of catalysts occur [12–14]. The phase of the healing agent changes from a mobilable liquid to hard material through polymerization, which in turn results in rebinding of the cracks with good mechanical properties. Herein, we have synthesized a polymethacrylate containing a photo responsive cinnamoyl group in the side chain, poly(2-cinnamoyloxyethyl methacrylate) (PCEMA), via a one-step polymer analogous reaction for use as a healable polymer (Figure 2.1.) [15–17]. Using the reversible photo crosslink and cleavage reactions between cinnamoyl groups by 365 and 254 nm UV irradiation, respectively, the surface hardness of the polymer film could be controlled.

2.2. Experimental

Materials and instruments

Ethyl methacrylate, butyl methacrylate, hexyl methacrylate, poly(2-hydroxyethyl methacrylate) (PHEMA), cinnamoyl chloride, hydrocinnamoyl chloride, and pyridine were purchased from Sigma-Aldrich Chemical Co. Azobisisobutyronitrile (AIBN) was purchased from TCI. All reagents and solvents were used without further purification. Polymer films (20–100-lm thick) were prepared by casting a 20 wt% solution of the samples in *N*-methyl-2-pyrrolidone onto a glass substrate. The films were then dried for 6 h at 40 °C and 12 h at 60 °C to remove residual solvent. Photo crosslinking was performed using a 4 W 365 nm UV lamp and photo cleavage was performed using a 4 W 254 nm UV lamp (Spectronics Corp., Westbury, NY, USA). In either case, the lamp was placed above the sample at a distance of 1 cm. ^{1}H NMR spectra (500 MHz) were measured in $CDCl_3$ using a Bruker Avance 500 instrument. The M_w and polydispersity index were obtained by gel permeation chromatography (GPC, Viscotek) using a diffractometer as the detector. THF was used as the solvent, and monodispersed polystyrene was used as the standards. Differential scanning calorimetry (DSC, TA Instruments 2920 differential scanning calorimeter) was carried out at heating and cooling rates of 5 °C min^{-1}. To eliminate the effect of thermal history on the sample transitions, all samples were heated to 200 °C and held at that temperature for 5 min before cooling. The transition temperatures and enthalpy changes were obtained from the second heating scan. Infrared (IR) spectra were recorded in the attenuated total reflectance (ATR) mode over the frequency range 4000–650 cm^{-1}, on a Nicolet 6700 instrument (Thermo Scientific, USA). Optical microscopy (OM) images were obtained with an optical microscope (ECLIPSE E600 POL, NIKON) equipped with a digital camera (COOLPIX E500, NIKON). Pencil scratch hardness was evaluated with Staedtler pencils (Mars Lumograph, Germany) with different hardness.

Preparation of poly(2-cinnamoyloxyethyl methacrylate) copolymer (PCEMA-#s)

A series of PCEMA-#s (where # is the mol% of monomeric units containing cinnamoyl side group, 10, 30, 50, 70, and 100) having different cinnamoyl side group contents were synthesized. The synthetic procedures for PCEMA-100 are provided here as an example. Cinnamoyl chloride (3 g, 18 mmol) was added to a stirred solution of PHEMA (2 g, 15.2 mmol) in 100 mL of pyridine under a nitrogen atmosphere. The reaction mixture was stirred at room temperature for 24 h and then poured into water. The precipitate was further purified by several precipitations from a THF solution into hexane, and then dried under vacuum at room temperature. Although the reaction conditions were mild, the degrees of substituted side group were higher than 99%. The ^{1}H nuclear magnetic resonance (NMR) spectra of PCEMA (CDCl3, d): 1.06 (m, 3H), 1.83 (m, 2H), 4.09 (m, 2H), 4.21 (m, 2H), 6.47 (m, 1H), 7.32 (m, 3H), 7.51 (m, 2H), and 7.61 (m, 1H). We calculated the degree of substitution using the ^{1}H NMR results by comparing the multiplet at 1.06 (3H) from the backbone and the multiplet at 6.47 (1H) from the cinnamoyl double bond.

2.3. Results and Discussion

The overall healing and surface hardness control process of the PCEMA is depicted in Figure 2.2. The exposure of PCEMA film to 365 nm UV light increases the surface hardness of the healable polymer film through the well-known [2 + 2] cycloaddition between cinnamoyl groups in the polymer side chains by the formation of crosslinked cinnamoyl groups. The subsequent exposure to 254 nm UV light led to photo cleavage to form the cinnamoyl groups, which can potentially impart healing properties on the damaged polymer film by making the polymer chains mobile through the thermal treatment. After thermal treatment above T_g of the polymer followed by the irradiation of 365 nm UV light, the damaged surface could be changed into a healed hard film. The damaged hard film was prepared by making micro-sized artificial cracks (width: 20–40 μm) on the film surface using a razor blade, and then the polymer was heated to 80 °C. We found that the chain mobility of the polymer is the key factor to give the healing property from the same healing tests using poly(n-alkyl methacrylate)s having different side chain lengths [18] and PCEMA derivatives having various contents of cinnamoyl group in the side chain (Figure 2.3.,2.4.). These polymers have different T_g values, and the healing properties were observed when each damaged polymer film was heated to ~20 °C higher than their respective T_g as expected. However, we could not observe any healing phenomena when only UV light of 254 and/or 365 nm wavelengths was irradiated onto the damaged polymer films. The healing properties of the polymer films were confirmed by optical microscope (OM) studies. In view of the best performance among the series of polymethacrylate derivatives, we selected PCEMA with almost 100% cinnamoyl group in the side chain, PCEMA-100, as a model polymer.

Figure 2.5(a) shows OM images of the PCEMA-100 films before (left) and after (right) thermal treatment at 80 °C for 24 h. Since the temperature for the thermal treatment is higher than 60.2 °C, the T_g of PCEMA-100, the polymer chains having sufficient chain mobility can induce the healing of the micro-sized cracks on the polymer film; the polymer chains could penetrate into the gaps of cracks, and then fill them up by the formation of chain entanglements without any chemical reactions. However, during the photo crosslinking reaction via the irradiation of 365 nm UV light for 24 h at room temperature, the healing behavior of the damaged PCEMA-100 films was not observed (Figure 2.5(b)). Although others have reported that the photo crosslinking reaction could assist the healing process in highly flexible environments such as in hydrogel or macromonomer systems [11,19,20], we could not observe the healing behavior, possibly because the chain mobility of PCEMA-100 is not enough to induce the inter-diffusion of the polymer chains into the cracks at room temperature. When the damaged films were heated to 80 °C upon the 365-nm UV irradiation for 24 h (Figure 2.5(c)), some slight healing phenomena were observed while complete healing could not be achieved. Since the UV light was irradiated simultaneously with the heat treatment, chains were mobile in the beginning of the process, while the crosslinking reactions by the UV limited the chain mobility resulting in the partial healing as shown in Figure 2.5(c). When the damaged PCEMA-100 film was heated at 80 °C after the irradiation of 365 nm UV light, no healing phenomena could be observed (data not shown). These results suggest that the photo crosslinking reaction between cinnamoyl groups in PCEMA-100 via 365 nm UV light decreases the chain mobility to produce PCEMA-100 film having hard surface, while this can interrupt the healing process due to the lack of the chain mobility. Therefore, UV light with 254 nm wavelength was irradiated onto photo crosslinked PCEMA-100 film having micro-sized cracks before the thermal treatment. We expected that this could increase the chain mobility of the crosslinked PCEMA-100 film, because 254 nm UV light can cleave the crosslinked cinnamoyl structures. After the 254 nm UV irradiation for 24 h, the damaged soft film was healed, and the subsequent 365 nm UV irradiation turned the soft healed film into a hard healed film by the photo crosslinking reactions. Figure 2.5(d) shows the damaged hard film and completely healed hard film produced through the healing process as illustrated in Figure 2.2; damaged hard film was softened with 254 nm UV light, healed by thermal treatment, and the surface re-hardened with 365 nm UV light. Since both thermal treatment and UV irradiation could be applied to a small area, this approach is a very promising method for practical applications.

Almost no change is seen for the ATR-IR spectra of the PCEMA-100 film between, before, and after the thermal treatment at 80 °C for 24 h, if any. A pristine PCEMA-100 film showed IR absorption bands of cinnamoyl C=O and C=C at 1713 and 1637 cm^{-1}, respectively (Figure 2.6(a)). Therefore, the cycloaddition and/or other unexpected chemical reactions did not occur by the thermal treatment (Figure 2.6(b)). This indicates that the inter-diffusion of polymer chains across the crack induced by the high mobility of polymer chains above T_g is a major factor for healing behavior, not chemical reaction. In contrast, the carbonyl C=O absorption band shifts to around 1725 cm^{-1} and C=C absorption bands disappears upon the irradiation of 365 nm UV light (Figure 2.6(c)). When PCEMA-100 was irradiated by 365 nm UV light, it became insoluble in common solvents ranging from very polar H_2O to nonpolar n-hexane and the films become harder, indicating that the photo crosslinking reaction between the cinnamoyl side groups in PCEMA-100 had successfully occurred [11]. The effects of photo crosslinking reactions on the mechanical properties of PCEMA-100 film were further confirmed by the surface hardness tests.

The surface hardness changes of PCEMA-100 film during the healing processes were determined by the pencil scratch method (Table 2.1) [21,22]. By the irradiation with 365 nm UV light, the scratch hardness of the pristine PCEMA-100 film increased from 2H to 4H, which is known to be sufficient for industrial applications [23]. When the photo crosslinked PCEMA-100 film was exposed to the 254 nm UV light for 15 min, the scratch hardness decreased to 3H, indicating the surface becomes softer by the photo cleavage reaction. The reason that surface hardness value of photo cleaved PCEMA-100 film is still higher than that of pristine PCEMA-100 film is thought to be the relatively low absorption efficiency of 254 nm UV light on the surface of the polymer film. Although the surface hardness did not completely decrease to 2H, it was found to be enough to provide the healing property of PCEMA-100 film by regaining some of the mobility of the polymer chain. When 254 nm UV light was irradiated for longer than 15 min, thenPCEMA-100 film became even harder due to the possible side radical reactions different from the photo crosslink reaction as reported by others [24,25] After the thermal treatment at 80 °C followed by the irradiation of 365 nm UV light, the surface hardness value of PCEMA-100 film increased again to 4H.

2.4. Conclusion

Healable polymethacrylate derivatives have been designed and synthesized by introducing photo crosslinkable cinnamoyl group into the side chain. The reversible photocycloaddition reaction via UV irradiation also provides hardness-controllable properties. With issues related to mechanical and healing properties, this concept of using hardness-controllable thermoplastic polymers as healable polymers opens the way for future exploration.

2.5. References

[1] D. Y. Wu, S. Meure, D. Solomon, Self-Healing Polymeric Materials: A Review of Recent Developments, Prog. Polym. Sci., 2008, 33, 479

[2] E. B. Murphy, F. Wudl, The World of Smart Healable Materials, Prog. Polym. Sci., 2010, 35, 223

[3] S. Burattini, B. W. Greenland, D. Chappell, H. M. Colquhoun, W. Hayes, Healable Polymeric Materials: A Tutorial Review, Chem. Soc. Rev., 2010, 39, 1973

[4] Y. H. Kim, R. P. Wool, A Theory of Healing at a Polymer–Polymer Interface, Macromolecules, 1983, 16, 1115

[5] O. J. Mcgarel, R. P. Wool, Craze Growth and Healing in Polystyrene, J. Polym. Sci. Polym. Phys., 1987, 25, 2541

[6] Y. M. Boiko, R. E. Prudhomme, Bonding at Symmetric Polymer/Polymer Interfaces Below the Glass Transition Temperature, Macromolecules, 1997, 30, 3708

[7] X. Chen, M. A. Dam, K. Ono, A. Mal, H. Shen, S. R. Nutt, K. Sheran, F. Wudl, A Thermally Re-mendable Cross- Linked Polymeric Material, Science, 2002, 295, 1698

[8] Q. Tian, Y. C. Yuan, M. Z. Rong, M. Q. Zhang, A Thermally Remendable

Epoxy Resin, J. Mater. Chem., 2009, 19, 1289

[9] Y. Zhang, A. A. Broekhuis, F. Picchioni, Thermally Self-Healing Polymeric Materials: The Next Step to Recycling Thermoset Polymers?, Macromolecules, 2009, 42, 1906

[10] B. Ghosh, M. W. Urban, Self-Repairing Oxetane-Substituted Chitosan Polyurethane Networks, Science, 2009, 323, 1458

[11] C. M. Chung, Y. S. Roh, S. Y. Cho, J. G. Kim, Crack Healing in Polymeric Materials via Photochemical [2 + 2] Cycloaddition, Chem. Mater., 2004, 16, 3982

[12] S. R. White, N. R. Sottos, P. H. Geubelle, J. S. Moore, M. R. Kessler, S. R. Sriram, E. N. Brown, S. Viswanathan, Autonomic Healing of Polymer Composites, Nature, 2001, 409, 794

[13] S. H. Cho, H. M. Andersson, S. R. White, N. R. Sottos, P. V. Braun, Polydimethylsiloxane-Based Self-Healing Materials, Adv. Mater., 2006, 18, 997

[14] K. S. Toohey, N. R. Sottos, J. A. Lewis, J. S. Moore, S. R. White, Self-Healing Materials with Microvascular Networks, Nat. Mater., 2007, 6, 581

[15] J. C. Lee, M. H. Litt, C. E. Rogers, Synthesis and Properties of Liquid Crystalline Polymers Containing an Oxyethylene Backbone and n-Octylsulfonylmethyl Side Groups, Macromolecules, 1998, 31, 2440

[16] J. S. Chung, B. G. Kim, E. H. Sohn, J. C. Lee, Molecular Structure and Surface Properties of Comb-Like Fluorinated Poly(oxyethylene)s Having Different Content of Fluoroalkyl Side Group, Macromolecules, 2010, 43, 10481

[17] E. H. Sohn, S. H. Kim, M. Lee, J. C. Lee, K. Song, Surface Properties and Liquid Crystal Alignment Behavior of Poly(2-Hydroxyethyl Methacrylate) Derivatives with Alkyl Ester Side Chains, J. Colloid Interf. Sci., 2011, 360, 623

[18] D. Kilburn, G. Dlubek, J. Pionteck, M. A. Alam, Free Volume in Poly(n-Alkyl Methacrylate)S From Positron Lifetime and PVT Experiments and Its Relation to the Structural Relaxation, Polymer, 2006, 47, 7774

[19] P. Froimowicz, H. Frey, K. Landfester, Towards the Generation of Self-Healing Materials by Means of a Reversible Photo-Induced Approach, Macromol. Rapid Commun., 2011, 32, 468

[20] S. Y. Cho, J. G. Kim, S. Y. Oh, C. M. Chung, Heat-Induced Crack Healing in a Perfluorocyclobutane-Containing Polymer, Macromol. Res., 2010, 18, 212

[21] P. R. Guevin, State-of-the-Art Instruments to Measure Coating Hardness, J. Coat. Technol., 1995, 67, 61

[22] Z. Chen, L. Y. L. Wu, E. Chwa, O. Tham, Scratch Resistance of Brittle

Thin Films on Compliant Substrates, Mater. Sci. Eng. A, 2008, 493, 292

[23] R. Ikeda, H. Tanaka, H. Uyama, S. Kobayashi, Enzymatic Synthesis and Curing of Poly(cardanol), Polym. J., 2000, 32, 589

[24] F. M. Andreopoulos, E. J. Beckman, A. J. Russell, Photoswitchable PEG-CA Hydrogels and Factors that Affect Their Photosensitivity, J. Polym. Sci. Part A Polym. Chem., 2000, 38, 1466

[25] Y. Chen, J. D. Wu, Preparation and Photoreaction of Copolymers Derived from N-(1-phenylethyl)acrylamide and 7-acryloyloxy-4-methyl Coumarin, J. Polym. Sci. Part A Polym. Chem., 1994, 32, 1867

Table 2.1. Surface hardness change of PCEMA-100 films during the healing processes.

λ [nm]	No irradiation	365	365/254	365/254/365
Scratch hardness	2 H	4 H	3 H	4 H

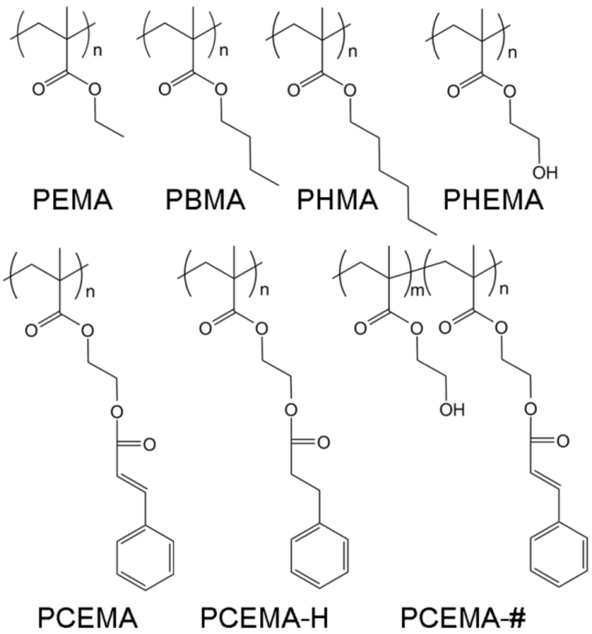

Figure 2.1. Representative chemical structure of the polymers used in this study.

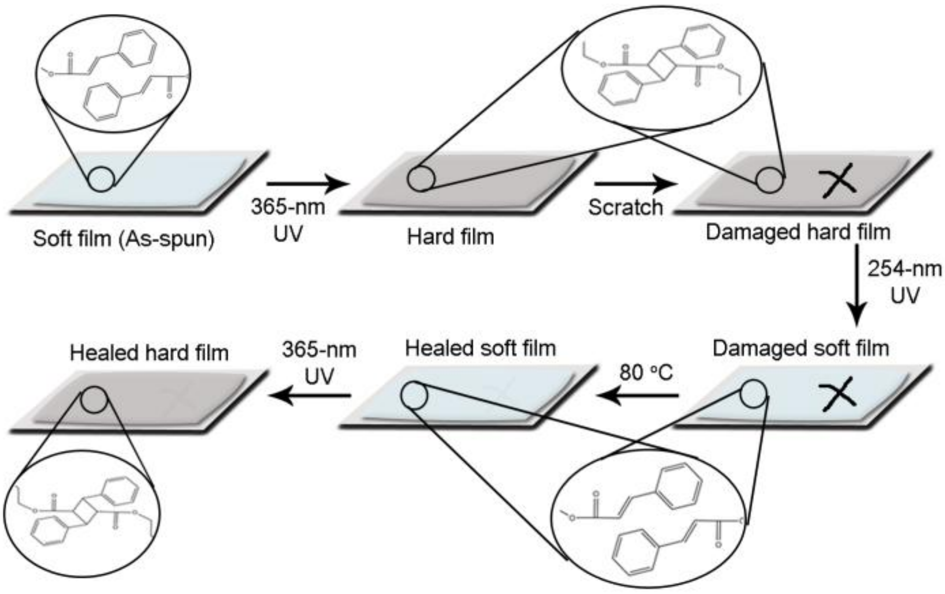

Figure 2.2. Schematic illustration of the facile healing processes of PCEMA film with controlling the surface hardness.

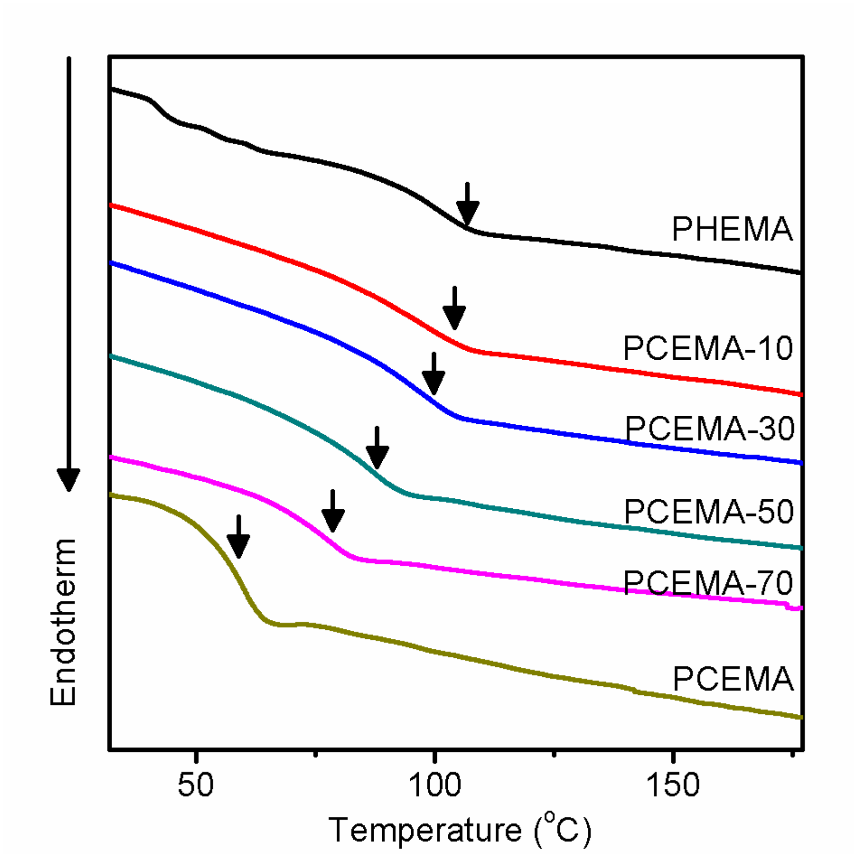

Figure 2.3. DSC curves of synthesized polymers. The black arrows indicate the glass transition temperature.

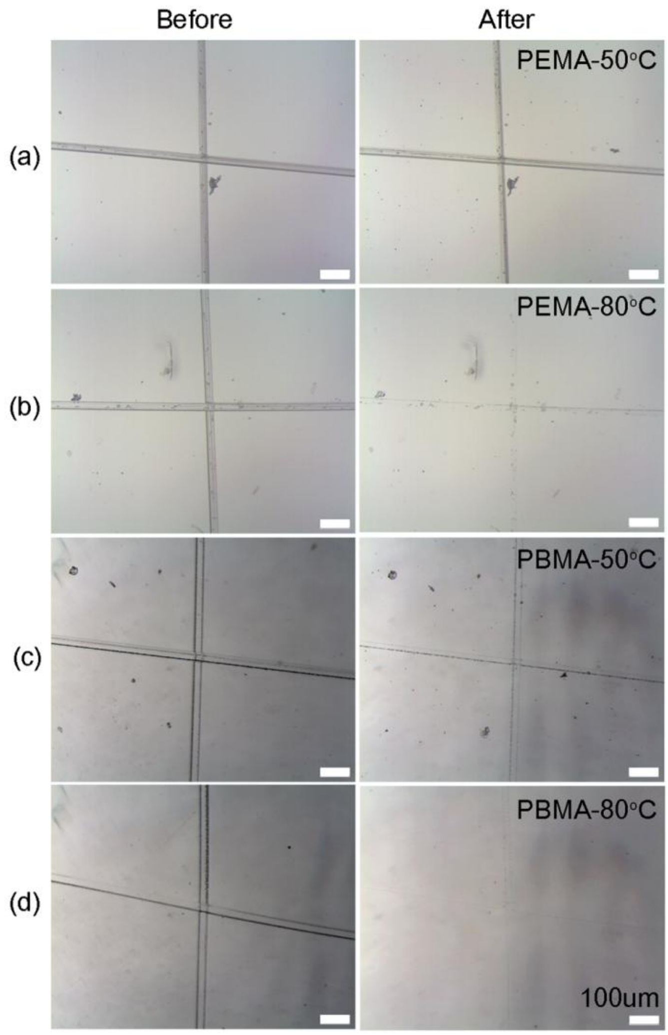

Figure 2.4. Optical micrographs of the PEMA films healed at (a) 50 °C and (b) 80 °C and the PBMA films healed at (c) 50 °C and (d) 80 °C.

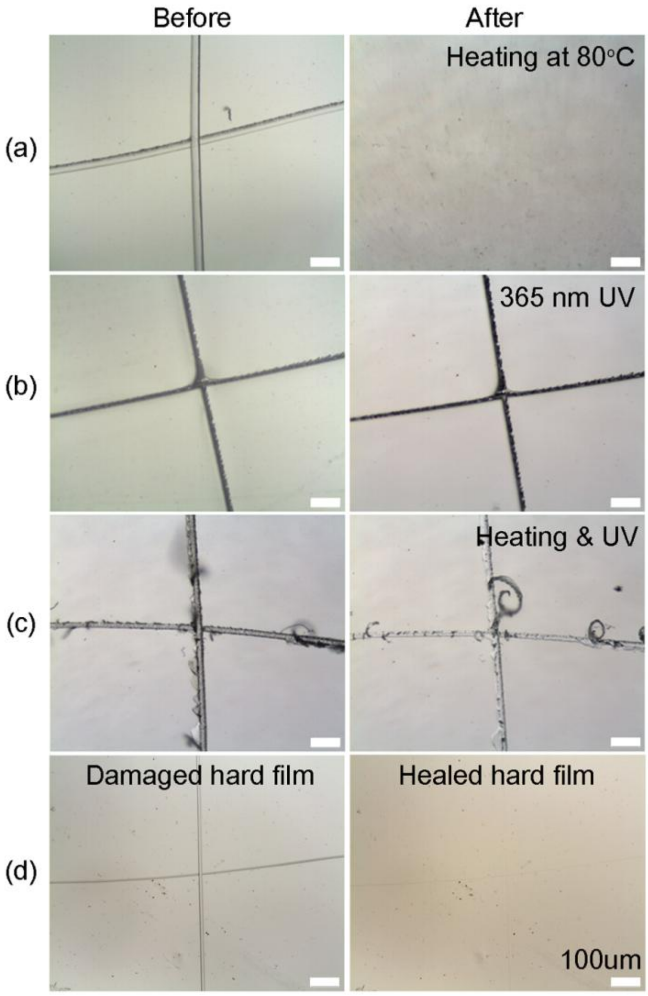

Figure 2.5. Comparison of optical micrographs of PCEMA-100 films before(left) and after(right) the healing processes, based on (a) thermal treatment, (b) 365 nm UV irradiation, (c) thermal treatment and 365 nm UV irradiation simultaneously, and (d) overall treatments as illustrated in Figure 2.2..

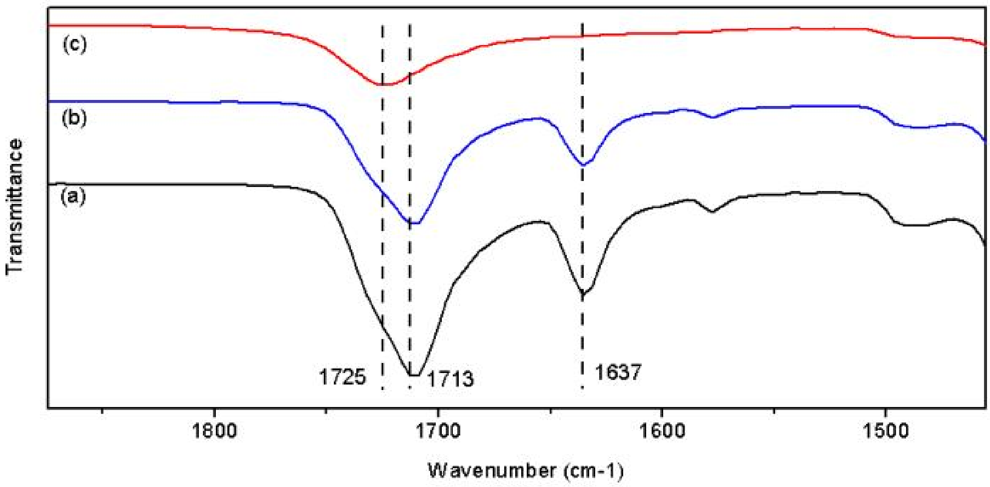

Figure 2.6. ATR-IR spectra of PCEMA-100: (a) pristine, (b) after thermal treatment at 80 °C for 24 hours, and (c) after 365 nm UV irradiation for 24 hours.

Chapter 3

The Study of Self-healing Property Change of Diels-Alder Based Polymeric Materials Affected by Reactivity of Furan Functionalities

3.1. Introduction

Recently, there has been increased demand of smart polymeric materials which have a specific response to external stimuli like heat, pressure, pH, et cetera. Among these stimuli responsive polymers, self-healable polymers, which can recover its pristine properties after micro/macroscale of physical damage, have drawn tremendous of interests because of its durable nature. Self-healing property can effectively increase stability and lifetime of polymeric materials which are vulnerable to long-term exposure to chemical/physical fatigue.

To obtain this self-healing property, two essential factors should be satisfied, interaction and mobility. First, there should be an interaction that can replace or recover the pristine internal interaction in polymer material. Second, to this interaction works, the materials should have enough mobility to fill the fracture void. Many researches have been made to design self-healing polymeric models which meet aforementioned two prerequisites, which include healing agent encapsulation[1-3], supramolecular interactions[4-5], covalent bonding, et cetera.[6-10]

Reversible covalent bonds have been utilized for self-healing materials due to its reversibility can induce repeatable self-healing. Furthermore, the mechanical properties of healed materials are preserved because chemical structures are identical to that of the original ones. Among these, Diels-Alder(DA) reaction is one of the most commonly exploited chemical reaction used in various chemical synthesis and applications.[11-13] This well understood [4+2] cycloaddition reaction between diene and dienophile could be easily reacted or cleaved(retro-Diels-Alder, rDA) by controlling the temperature without any catalyst or other external stimuli. Application of the DA reaction in self-healing materials have been widely studied due to aforementioned advantages.[14-17] Yet, to the best of our knowledge, there is no study about the influence of the reactivity of Diels-Alder reaction on healing efficiency. In this report, self-healable polymethacrylates having furan functionalities with different electron density were synthesized and characterized. The reactivity of synthesized polymers with maleimide cross-linker and the self-healing property of prepared DA polymer network were studied by various experiments.

3.2. Experimental

Materials

Furfuryl alcohol (FA; 98%), poly(ethylene glycol) methyl ether methacrylate(PEGMMA; average Mn=500, contains 100 ppm MEHQ and 200 ppm BHT as inhibitor) dibutyltin dilaurate (95%), 1,1'-(methylenedi-4,1-phenylene)bismaleimide (bM; 95%) and 2-hydroxyl ethyl methacrylate(HEMA; contains 250 ppm monomethyl ether hydroquinone as inhibitor, 97%) were purchased from Sigma-Aldrich and used as received. 2-furyloyl chloride (FC; 98%) and 2-isocyanato ethyl methacrylate (NCO-MA, stabilized with BHT; 98%) were purchased from Tokyo chemical industry and used as received. α,α'-Azobis(isobutyronitrile) (AIBN; 98%) was purchased from Tokyo chemical industry and recrystallized with ethanol before used. Methylene chloride (MC), dimethylformamide (DMF), tetrahydrofuran (THF), n-hexane, chloroform, diethyl ether and pyridine (99.5%) were purchased from Daejung Chemicals and used after dehydrated with molecular sieve.

Synthesis of electron-deficient furan-functionalized monomer

(dFMA)

FC (202 mmol, 26.48 g) diluted with MC (100 mL) was added to a stirred solution of HEMA (243 mmol, 31.65 g) and pyridine (243 mmol, 19.17 g) in 200 mL of MC at 0 °C. The reaction mixture was stirred at RT for 24 hours. Afterwards, product was poured into separatory funnel with water and washed several times. The organic layer was then dried over anhydrous sodium sulfate and filtered. Remained product solution was evaporated under reduced pressure to remove solvent. ^{1}H NMR (400 Hz, $CDCl_3$, ppm, δ): 7.61 (s, 1H), 7.21 (d, 1H) and 6.53 (d, 1H), 6.14 (s, 1H), 5.60 (s, 1H), 4.53(t, 2H), 4.47(t, 2H), 1.95(s, 3H).

Synthesis of electron-rich furan functionalized monomer (rFMA)

NCO-MA (71 mmol, 10.98 g), FA (106 mmol, 10.44 g) and a few drops of dibutyltin dilaurate were dissolved in 200 mL of chloroform and stirred at 50 °C for 24 hours. Afterwards, product was poured into separatory funnel with water and washed several times. The organic layer was then dried over anhydrous sodium sulfate and filtered. Remained product solution was evaporated under reduced pressure to remove solvent. ^{1}H NMR (400 Hz, CDCl3, ppm, δ): 7.41 (s, 1H), 6.40 (d, 1H), 6.34 (d, 1H), 6.10(s, 1H), 5.58(s, 1H), 5.05(s, 2H), 4.22(t, 2H), 3.50(t, 2H), 1.93(s, 3H).

Polymerization of poly(furoyl methacrylate)-co-poly(poly(ethylene glycol) methyl ether methacrylate) (dPFMA)

A series of poly(furoyl methacrylate)-co-poly(poly(ethylene glycol) methyl ether methacrylate) (dPFMA#s, where # is the mol% of furoyl methacrylate) having different furan side group contents were synthesized by adjusting the feed ratio of monomers. The synthetic procedures for dPFMA6 are provided here as an example. dFMA (60 mmol, 13.44 g), PEGMA (40 mmol, 20.00 g) and AIBN(0.5 wt% of dFMA) in 334 mL of THF were taken in a three-necked round bottom flask. The mixture was stirred at reflux for 4 hours and then poured into n-hexane. The precipitant was filtered and dried.

Polymerization of poly(furfuryl methacrylate)-co-poly(poly(ethylene glycol) methyl ether methacrylate) (rPFMA)

A series of poly(furfuryl methacrylate)-co-poly(poly(ethylene glycol) methyl ether methacrylate) (rPFMA#s, where # is the mol% of furfuryl methacrylate) having different furan side group contents were synthesized by adjusting the ratio of monomers. The synthetic procedures for rPFMA6 are provided here as an example. rFMA (60 mmol, 15.20 g), PEGMA (40 mmol, 20.00 g) and AIBN(1 wt% of rFMA) in 352 mL of THF were taken in a three-necked round bottom flask. The mixture was stirred at reflux for 4 hours and then poured into diethyl ether. The precipitant was filtered and dried.

Preparation of cross-linked polymer film

Synthesized polymers and bM cross-linker (furan/maleimide molar ratio = 1:1) were dissolved into DMF to make 10% solution. Solution was poured onto silicon mold (70 mm × 12 mm) and dried in air at 120 °C for 24 hours. Then the film was heated in air at 60 °C for 24 hours to prepare cross-linked polymer film (bM-rPFMA# and bM-dPFMA#).

Healing efficiency test

A rectangular test specimen obtained from cross-linked polymer film preparation step was damaged by tapping with 5 mm wide razor blade at RT. 5 mm wide hole was made by full-penetration of razor blade. Crack healing experiment was performed at 120 °C for 1 hour and 60 °C for 24 hours in air. Second crack was formed at the same area which the first crack was formed, and the healing procedure was identical with the first one.

Preparation of monofunctionalized maleimide (mM)

4-(2-Hydroxyethyl)-10-oxa-4-azatricyclo[5.2.1.02,6]dec-8-ene-3,5-dione (protected hydroxyethyl maleimide) was synthesized according to the literature [18]. Purified protected hydroxyethyl maleimide was dissolved in DMF and stirred at 120 °C for 3 hours. Solution was then poured into diethyl ether and filtered. Yellow powder was obtained after removal of the solvent under reduced pressure. ^{1}H NMR (400 Hz, DMSO-d_6, ppm, δ): 7.01 (s, 2H), 3.47(t, 2H), 3.39(t, 2H).

Kinetics

An equivalent molar mixture of dPFMA6/rPFMA6 and mM was dissolved in THF and the solvent was removed by rotary evaporation under reduced pressure at 30 °C for 30 minutes. Then the homogeneous mixture was obtained at specific time intervals at 60 °C and quickly dissolved in deuterated dimethylsulfoxide and then sealed in a glass tube to calculate the DA reaction conversion via ^{1}H NMR.

Characterization

^1H NMR spectra were measured using an Avance-400 spectrometer (Bruker). The M_w and polydispersity index were obtained by gel permeation chromatography (GPC, Viscotek). THF was used as the solvent and monodispersed polystyrene was used as the standards. Differential scanning calorimetry (DSC, DSC N-650, Scinco) was carried out at heating and cooling rated of 10 °C min^{-1} under nitrogen. Infrared (IR) spectra were recorded in the attenuated total reflectance (ATR) mode over the frequency range 4000-400 cm^{-1}, on an ALPHA-P (Bruker). Optical microscopy (OM) images were obtained with an optical microscope (DIMIS-M). Pencil scratch hardness was evaluated with Staedtler pencils (Mars Lumograph, Germany) with different hardness. Mechanical properties were obtained with a universal testing machine QM100S (Qmesys) with elongation rate of 10 mm min^{-1} at RT.

3.3. Results and Discussion

Preparation of furan functionalized methacrylates

Furan-functionalized monomers (dFMA and rFMA) which have different electron density of furan moiety were synthesized according to Figure 3.1. dFMA was obtained from treating HEMA with FC in the presence of pyridine and rFMA was obtained from treating NCO-MA with FA in the presence of tin catalyst. dFMA has relatively electron-deficient furan functionality compared with rFMA due to the adjacent carbonyl group which is a strong electron-withdrawing group. Both reactions were characterized with ^{1}H NMR.

Furan-functionalized methacrylates(dPFMA and rPFMA) were then polymerized via free radical polymerization of furan-functionalized monomers(dFMA and rFMA) and PEGMA. The ratio of furan-functionalized monomers to PEGMA was 10/0, 6/4, 4/6, or 0/10 and the structure of dPFMA6 was confirmed via ^{1}H NMR as shown in Figure 3.2(A). The characteristic peaks at 7.62, 7.21 and 6.52 ppm are due to the furan moiety. The peaks at 6.15 and 5.60 ppm of double bond resonance of dFMA were disappeared and the peaks at 1.96-0.88 ppm of methacrylate backbone appeared. The structure of rPFMA6 was also confirmed via ^{1}H NMR as shown in Figure 3.2(B). The peaks at 7.42, 6.41 and 6.35 ppm are due to the furan moiety. The peaks at 6.10 and 5.58 ppm of double bond resonance of rFMA were disappeared and the peaks at 1.80-0.86 ppm of methacrylate backbone appeared. The structure of dPFMA6 and rPFMA6 was confirmed successfully and the ratio between furan-functionalized monomers and PEGMA in the synthesized polymer was calculated (Table 3.1). Product ratio of rPFMA6 was different from the one of dPFMA6 due to different reactivity of monomers, but the difference was not critical enough to bring out significant difference of chemical or mechanical properties. Molecular weight and PDI values of synthesized polymers are controlled to a similar level. The M_w values and PDI values are calculated by GPC analysis.

Self-healing property of bM-dPFMA

Cross-linked polymer film was obtained from DA reaction between furan-functionalized polymers and bismaleimide cross-linker. Equivalent amount of dPFMAs and bM solution was prepared and casted on the slide glass. After evaporation of solvent, bM-dPFMA cross-linked film was obtained and the self-healing behavior was examined by optical microscopy (Figure 3.3). The artificial cut of 20-40 width on the film surface of bM-dPFMA10, bM-dPFMA6, bM-dPFMA4 and bM-dPFMA0 was made using a razor blade and was shown in Figure 3.3(A-D). After healing process of heating at 120 °C for 1 hour and at

60 °C for 24 hours, the bM-dPFMA films exhibited different healing properties (Figure 3.3(E-H)). Crack on the surface of bM-dPFMA6 was healed completely after healing process, while others were healed partially.

The overall healing process of the bM-dPFMA was depicted in Figure 3.4. Cross-linked film cannot be healed due to its lack of mobility, while healing property can be obtained from the chain movement and entanglement at elevated temperature over its glass transition temperature.[19] After the film was damaged by razor blade, the film was heated at 120 °C to trigger the rDA reaction. Cleaved bM and dPFMA has enough mobility to fill the fracture void at elevated temperature and the DA reaction can be conducted after decreasing the temperature to 60 °C. With increasing the content of PEGMA, the mobility of polymer increases due to its low glass transition temperature. But without dPFMA, healing ability decreases due to the absence of chemical reaction at the crack void. There is an optimal point of ratio of monomers that can meet both healing ability and chain mobility.

Table 3.2 shows the surface hardness of bM-dPFMA films at room temperature. With increasing the content of dPFMA, mechanical strength of polymer increases drastically due to DA reaction with bM cross-linker. With considering both healing ability and mechanical property, bM-dPFMA6 was selected for further investigation. And for comparison, bM-rPFMA6 was also selected due to its similarities.

Thermal reversibility

The thermal reversibility of DA reaction of bM-dPFMA6 and bM-rPFMA6 was studied from the FT-IR spectra shown in Figure 3.5. As can be seen in Figure 3.5(A), the absorption peaks at 1581 and 1569 cm^{-1} of double bond of furan and maleimide are observed due to rDA reaction at 120 °C (black line - bM-dPFMA6_rDA 1^{st} cycle). The peaks were decreased after treating the sample for 24 hours at 60 °C (red line – bM-dPFMA6_DA 1^{st} cycle) and increased again after treating the sample for 1 hour at 120 °C (green line – bM-dPFMA6_rDA 2^{nd} cycle). Similar phenomena were occurred for bM-rPFMA6 sample (Figure 3.5(B)), the absorption peaks at 1601 and 1585 cm^{-1} observed at 120 °C (black line – bM-rPFMA6_rDA 1^{st} cycle) were disappeared at 60 °C (red line – bM-rPFMA6_DA 1^{st} cycle) and appeared again at 120 °C (green line – bM-rPFMA6_rDA 2^{nd} cycle) due to reversible DA/rDA reaction. This result indicates thermal reversibility of prepared polymers clearly, even though the DA reaction of bM-dPFMA6 was not conducted completely while that of bM-rPFMA6 was almost perfect, as can be seen in the red line in Figure 3.5(A).

DSC measurement was also used to confirm the DA/rDA reaction. 3 DSC cycles of repeated heating and cooling cycles ranged between 30 °C and 150 °C for each bM-dPFMA6 and bM-rPFMA6 samples are shown in Figure 3.6. As shown in Figure 3.6(A), the first heating scans showed a broad endothermic behavior above 100 °C, which indicates rDA reaction of bM-dPFMA6. During the cooling cycle, broad exothermic behavior was observed over below 80 °C which indicates DA reaction of cleaved furan and maleimide. DA/rDA reaction was observed repeatedly in the second and third cycle. DSC profiles of bM-rPFMA6 also showed similar thermal behavior during 3 cycles of repeated heating and cooling cycles (Figure 3.6(B)).

Self-healing efficiency

The self-healing behavior of bM-dPFMA6 and bM-rPFMA6 was studied by calculating the healing efficiency obtained through the measurement of the mechanical strength of the original, damaged, and healed film. The healing efficiency was calculated from eq. (1)

$$\text{Healing efficiency (\%)} = \frac{E_h - E_d}{E_o - E_d} \times 100 \tag{1}$$

where E_h is the elongation of the healed samples, E_d is the elongation of the damaged samples and E_o is the elongation of the original samples.

Figure 3.7 shows the stress-strain curves of the original, damaged, and healed samples of bM-dPFMA6 and bM-rPFMA6 films. For the first healing process, the healing efficiency of 36.09% for bM-dPFMA6 and 91.09% for bM-rPFMA6 was calculated from stress-strain curves. The healing efficiencies of bM-rPFMA6 were significantly higher than that of bM-dPFMA6 due to the reactivity difference of furan functionalities. This tendency was also observed for the second healing process, the efficiency was 17.49% for bM-dPFMA6 and 36.93% for bM-rPFMA6 films. The healing efficiency of second healing process was increased to 27.79% for bM-dPFMA6 and 88.75% for bM-rPFMA6 after 48 hours of heating. Both polymers showed their repeatable healing ability due to the chain mobility at elevated temperature and reversible DA reaction, but the efficiencies were significantly different.

Kinetic study

To investigate the influence of reactivity of furan functionality to healing efficiency, the kinetic study of DA reaction of dPFMA6 and rPFMA6 with maleimide was designed and performed by monitoring of ^{1}H-NMR spectra. mM was used as a maleimide to prevent intermolecular cross-linking reaction, which can inhibit the monitoring of ^{1}H-NMR spectra. In figure 3.8, the ratio between the integrated peak of proton (A) of unreacted dPFMA6 and proton (A') of reacted dPFMA6-mM adduct was calculated at different time intervals. The time-dependent reaction conversion of DA adduct, x, can be calculated from eq. (2).

$$\mathrm{x} = \frac{\text{Integral area of A}'}{\text{Integral area of A}'+\text{A}} \quad (2)$$

Since DA reaction of dPFMA6 and mM follows the second order kinetics [7], the rate equation can be obtained from eq. (3).

$$\frac{1}{1-\mathrm{x}} = k\mathrm{t} \quad (3)$$

The rate constant k for DA reaction of dPFMA and rPFMA6 with mM are shown in Figure 3.9. The k value of rPFMA6 was 0.5515 $dm^3mol^{-1}s^{-1}$, which was 24 times higher than that of dPFMA6, 0.0223 $dm^3mol^{-1}s^{-1}$. Additionally, the reaction conversion of dPFMA6 and rPFMA6 with mM are shown in Figure 3.10. The conversion of dPFMA6 was 31.5% at 24 h, while the conversion of rPFMA6 was 78.9% for the same time. According to the result, the reaction rate and conversion of DA reaction of rPFMA6 are significantly higher than those of dPFMA6. Since the DA reaction is normally a pericyclic reaction between electron-rich diene and electron-deficient dienophile, the electron-withdrawing carbonyl group adjust to the furan functionality of dPFMA can impede the DA reaction, which leads to the retarded healing efficiency of bM-dPFMA6.

3.4. Conclusion

A series of furan-functionalized methacrylates which have different content and electron density of furan moieties were synthesized and characterized. DA/rDA reaction between synthesized polymer and maleimide cross-linker was performed and characterized. DA polymer adduct can easily form free-standing film and its self-healing property was studied. Reactivity of DA reaction was varied with electron density of furan moieties and thus brought difference of self-healing efficiencies significantly. Delicate design of furan-functionalized polymer and proper use of this chemistry will bring out improved DA based self-healable polymeric materials with enhanced mechanical properties and self-healing properties.

3.5. References

[1] S. R. White, N. R. Sottos, P. H. Geubelle, J. S. Moore, M. R. Kessler, S. R. Siram, E. N. Brown, and S. Viswanathan, Nature, 2001, 409, 794.

[2] S. H. Cho, H. M. Andersson, S. R. White, N. R. Sottos, and P. V. Braun, Adv. Mater., 2006, 18, 997.

[3] K. S. Toohey, N. R. Sottos, J. A. Lewis, J. S. Moore, and S. R. White, Nat. Mater., 2007, 6, 581.

[4] P. Cordier, F. Tournilhac, C. Soulie-Ziakovic, and L. Leibler, Nature, 2008, 451, 977.

[5] J. Cui and A. del Campo, Chem. Commun., 2012, 48, 9302.

[6] X. Chen, M. A. Dam, K. Ono, A. Mal, H. Shen, S. R. Nutt, K. Sheran, and F. Wudl, Science, 2002, 295, 1698.

[7] A. A. Kavitha and N. K. Singha, ACS Appl. Mater. Interfaces, 2009, 7, 1427.

[8] H. M. Klukovich, Z. S. Kean, S. T. Iacono, and S. L. Craig, J. Am. Chem. Soc., 2011, 133, 17882.

[9] C. M. Chung, Y. S. Roh, S. Y. Cho, and J. G. Kim, Chem. Mater., 2004, 16, 3982.

[10] J. A. Yoon, J. Kamada, K. Koynov, J. Mohin, R. Nicolay, Y. Zhang, A. C.

Balazs, T. Kowalewski, and K. Matyjaszewski, Macromolecules, 2012, 45, 142.

[11] I. Kosif, E.-J. Park, R. Sanyal, and A. Sanyal, Macromolecules, 2010, 43, 4140.

[12] J. Li, M. Li, L -L. Zhou, S.-Y. Lang, H.-Y. Lu, D. Wang, C.-F. Chen, and L.-J. Wan, J. Am. Chem. Soc., 2016, 138, 7448.

[13] P. T. Dirlam, G. A. Strange, J. A. Orlicki, E. D. Wetzel, and P. J. Costanzo, Langmuir, 2010, 26, 3942.

[14] G. Zhang, Q. Zhao, L. Yang, W. Zou, X. Xi, and T. Xie, ACS Macro Lett., 2016, 5, 805.

[15] G. B. Lyon, A. Baranek, and C. N. Bowman, Adv. Funct. Mater., 2016, 26, 1477.

[16] Z. Gou, Y. Zuo, and S. Feng, RSC Adv., 2016, 6, 73140.

[17] A. A. Kavitha and N. K. Singha, Macromolecules, 2010, 43, 3193.

[18] G. Mantovani, F. Lecolley, L. Tao, D. M. Haddleton, J. Clerx, J. J. L. M. Cornelissen and K Velonia, J. Am. Chem. Soc., 2005, 127, 2966.

[19] W. J. Choi, J.-S. Chung, J. Kim, S.-K. Kim, S.-H. Cha, M. Park, and J.-C. Lee, *J. Coat. Technol. Res.*, 2014, **11**, 455.

Table 3.1. Characterization of dPFMA6 and rPFMA6

Samples	Feed ratio [X[a] : PEGMA]	Product ratio[b] [X[a] : PEGMA]	M_w[c] ($\times 10^4$, RID)	PDI[c]
dPFMA6	6 : 4	5.98 : 4.02	1.9	1.51
rPFMA6	6 : 4	5.75 : 4.25	1.7	1.39

[a] Furan functionalized monomer(dFMA or rFMA). [b] Composition of X *versus* PEGMA determined by ^{1}H NMR. [c] Determined by GPC using refractive index detector (RID) and calibrated with linear polystyrene standards (THF).

Table 3.2. Surface hardness of bM-dPFMA film

Samples	bM-dPFMA10	bM-dPFMA6	bM-dPFMA4	bM-dPFMA0
Scratch hardness	6H	3H	4B	7B

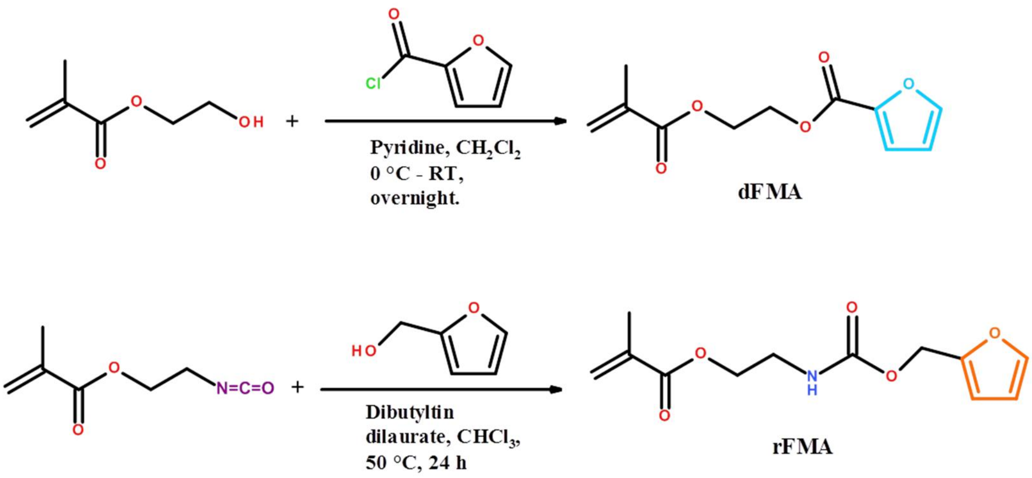

Figure 3.1. Synthesis of furan-functionalized monomers

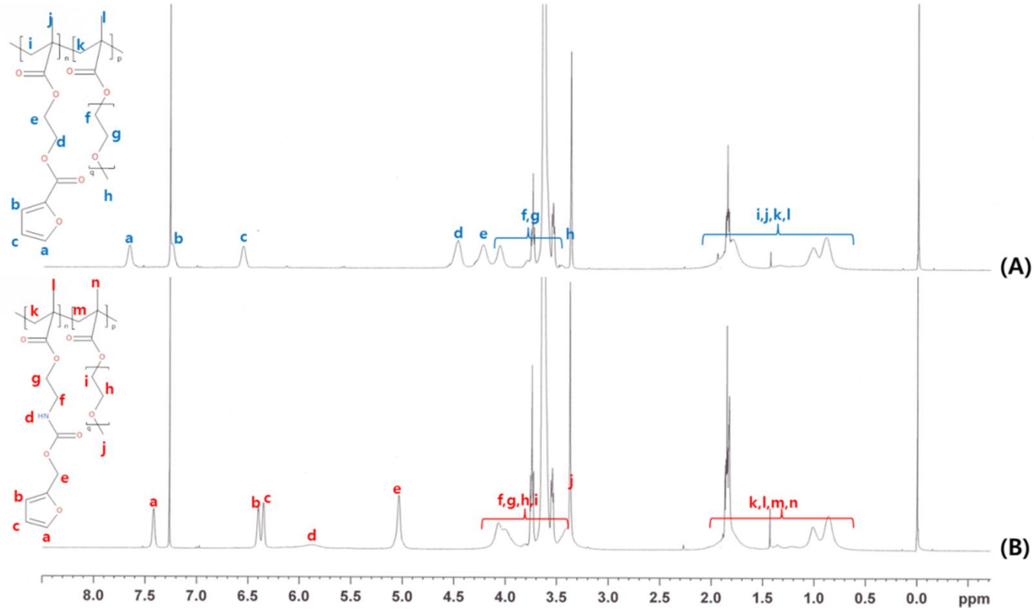

Figure 3.2. ^{1}H NMR spectra of the (A) dPFMA6 and (B) rPFMA6.

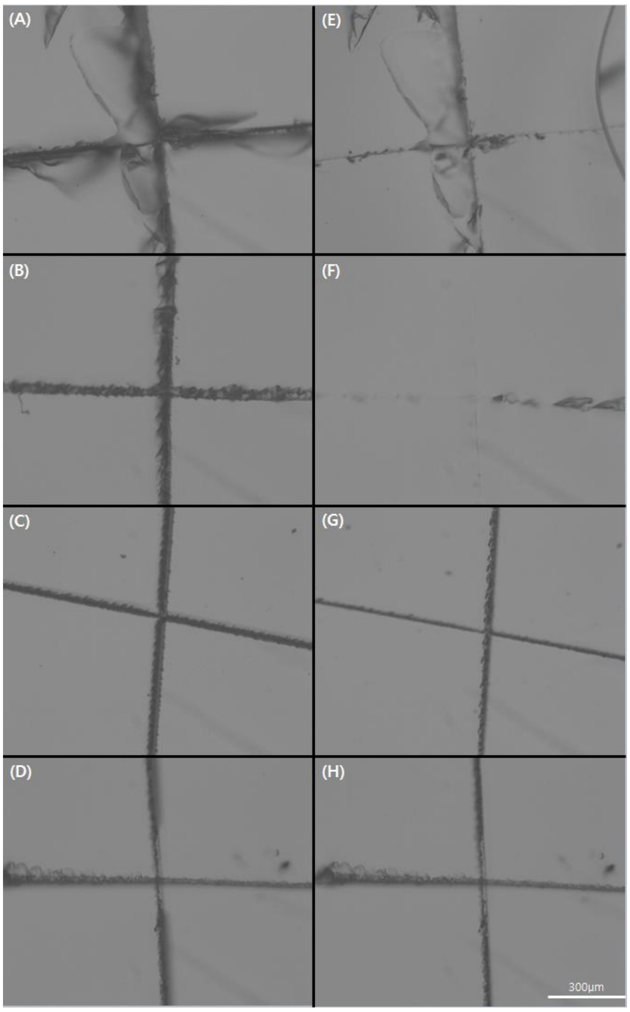

Figure 3.3. Optical microscopy images of damaged bM-dPFMA10, bM-dPFMA6, bM-dPFMA4 and dPFMA0 (A-D) and treated at 120 °C for 60 min and 60 °C for 24h (E-H).

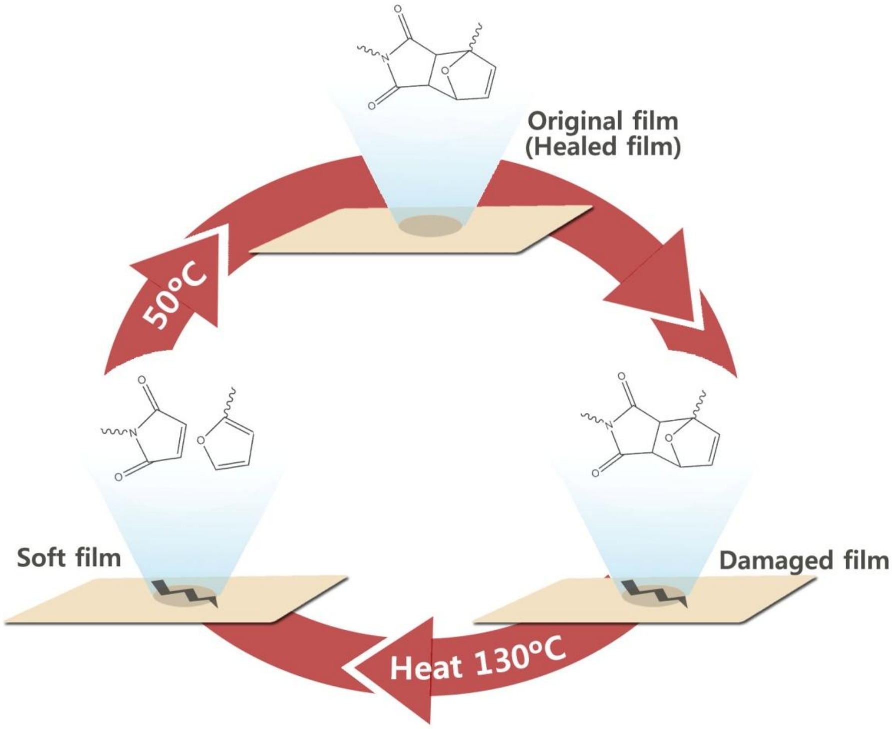

Figure 3.4. Schematic image of self-healing process of Diels-Alder based polymeric material.

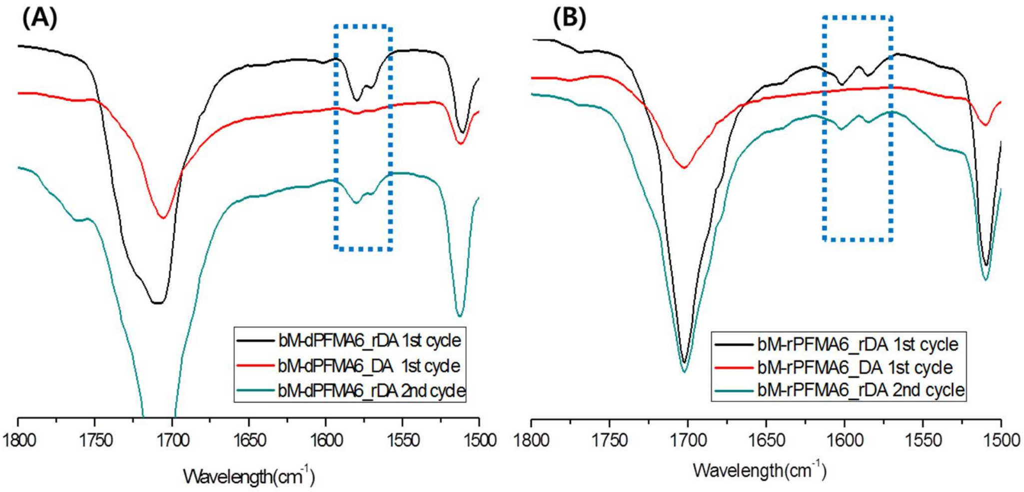

Figure 3.5. FT-IR spectra of bM-dPFMA6 (A) and bM-rPFMA6 (B).

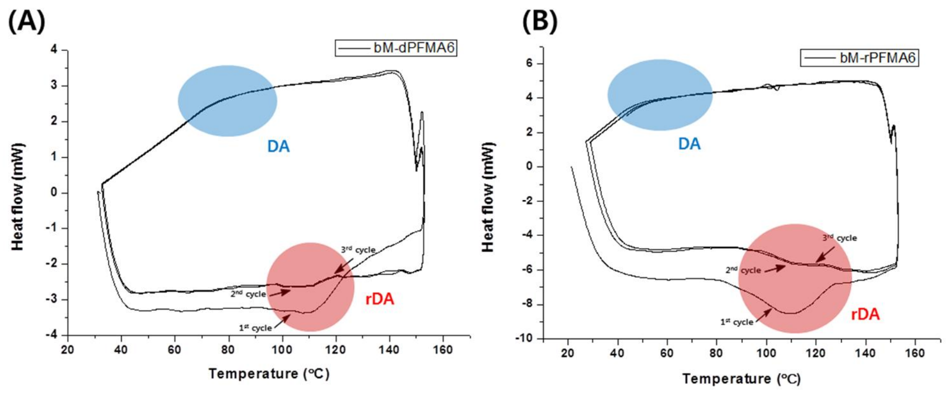

Figure 3.6. Repeated DSC curves of bM-dPFMA6 (A) and bM-rPFMA6 (B).

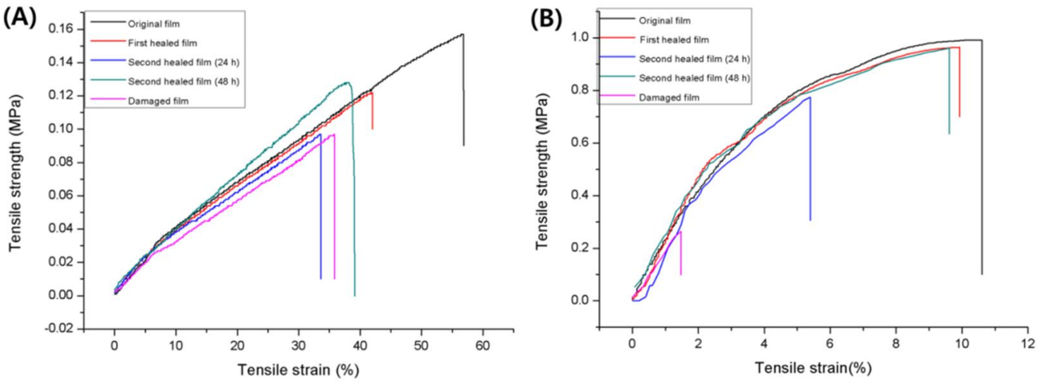

Figure 3.7. Stress-strain curves of original, damaged and healed samples of bM-dPFMA6 (A) and the bM-rPFMA6 (B).

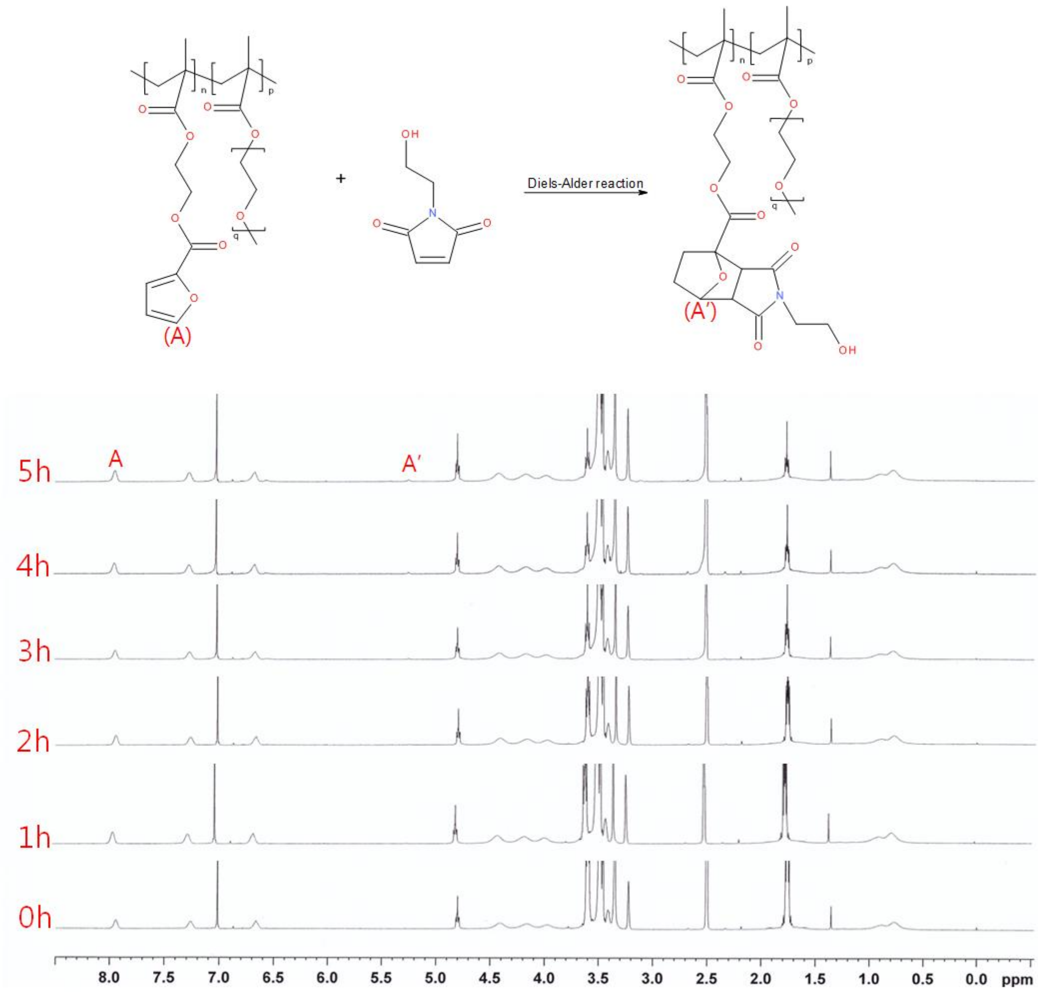

Figure 3.8. ¹H-NMR spectra of the mixture of dPFMA6 and mM kept at 60 °C for 0 to 5h.

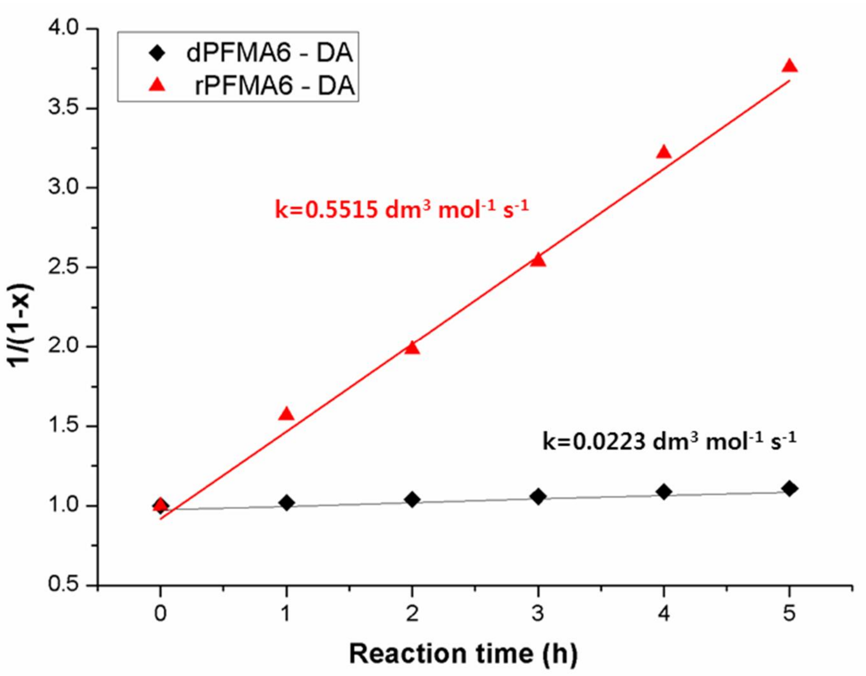

Figure 3.9. Second-order kinetic plot for the DA reaction between mM and dPFMA6/rPFMA6 at 60 °C.

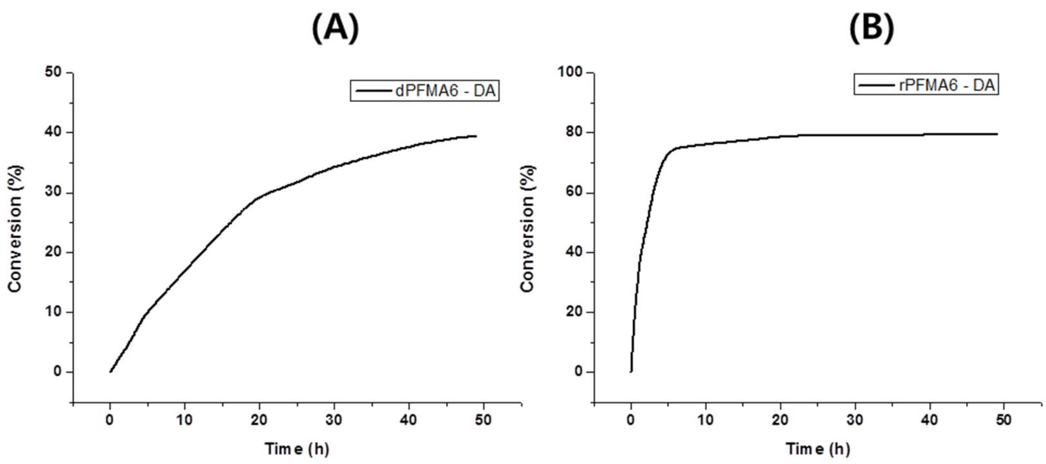

Figure 3.10. Conversion *versus* time plot of DA adduct between dPFMA6 and mM (A) and between rPFMA6 and mM (B).

Chapter 4

Fluoroalkyl-functionalized Graphene Oxide/Nafion Composite Membrane for All-Vanadium Redox Flow Battery

4.1. Introduction

There has Among the various redox flow battery (RFB) systems researched, the all-vanadium redox flow battery (VRFB) has drawn tremendous of interests due to its recyclability of electrolytes, long cycle life and non-toxic nature [1-3]. Since the separation of redox species of electrolytes, V(II)/V(III) for analyte and V(IV)/V(V) for catholyte, is crucial to maintain the cell performance during long-term operation, development of improved ion exchange membrane with enhaced ion selectivity has been a key issue [4-5].

Nafion membrane is the most reasonable choice among ion exchange membranes until today due to its excellent chemical stability and proton conductivity. However the large size of ion conducting channel of Nafion have limited its performances for RFBs due to the permeation of redox species.

Since the controlling of ion selectivity was the key issue to improve the performances of Nafion membranes, various methods have tried. Composite membrane was one of them, the permeation of redox species was controlled effectively by incorporating organic/inorganic fillers into Nafion matrix[6-

7]. In a few researches about application of graphene oxide (GO), have been utilized for various applications due to its physical/dimensional stability, ease of modification and unique strucrue [8-10], as a filler of ion exchange membranes for redox flow battery, GO can effectively decrease the permeation of actives species, especially vanadium, by acting as a barrier blocking hydrophilic channel, a main pathway of ion transport [11-13]. Despite of the aforementioned results, reports about graphene derivatives in RFB applications were very limited [14-15].

In this study, we modified GO with perfluoroalkyl chain to enhance the compatibility with Nafion (Figure 4.1(a)). We expect that hydrophilic channel of Nafion can be partially blocked in Nafion/GO composite membrane (N/GO) by the barrier effect of introduced GO, while the hydrophilic channel of Nafion/FGO composite membrane (N/FGO) can be narrowly and densely formed, also partially blocked, due to the influence of perfluoroalkyl chain of FGO to formation of microstructure in membrane preparation step (Figure 4.1(b)). Physical/electrochemical properties and VRFB cell performances of recast Nafion, N/GOs and N/FGOs were investigated in detail.

4.2. Experimental

Synthesis of fluoroalkyl chain-functionalized GO (FGO)

Graphite was supplied from BASF Korea and graphine oxide (GO) was prepared using graphite via modified Hummer's method [16]. 0.1 g of GO were dispersed in 70 mL of dimethylformamide (DMF, purchased from Daejung Chemicals, used after dehydrated with molecular sieve) and 4 g of 157 FS-L (Krytox acid, purchased from DuPont) and 4-(dimethylamino) pyridine (DMAP, purchased from Alfa aesar) were dissolved in 15 mL of DMF each. Prepared mixture and solutions were put into round bottom flask with magnetic stirring bar and condenser at 80 °C. Reaction was conducted at 120 °C for 20 hours at nitrogen atmosphere and the reaction mixture was diluted with water and filtered using anodic aluminium oxide filter. Product was obtained after drying at vacuum oven for several days.

Preparation of composite membranes

Prepared GO (0.1, 0.5, 1, 3, 5 wt%)was dispersed in 20 wt% of Nafion solution (purchased from Nano Getters) and casted on glass plate. After drying at 60 °C for

4 hours and 80 °C for 20 hours, membrane was washed with water and immersed in 1M H_2SO_4 solution for 24 hours. N/GO #s were obtained after drying in a vacuum oven, while # indicates the weight percent of GO content. Preparation process of N/FGO was identical with N/GO.

Characterization and VRFB cell tests

Infrared (IR) spectra were recorded using an ALPHA-P (Bruker) in the attenuated total reflectance (ATR) mode over the frequency range of 4000-400 cm^{-1}. Thermogravimetric analysis (TGA) was performed using TA instruments Thermogravimetric Analyzer 2050 with heating rate of 10 °C over 30 °C-700 °C. Proton conductivity was measured at RT under fully hydrated condition using ZAHNER IM-6ex impedance analyzer. Water uptake and volume swelling ratio was measured at RT under fully hydrated condition as shown in literature [17]. Vanadium permeability was measured by the method described in literature [18]. Diffusion cell was prepared with the membrane sandwiched between two half-cells, and the left half-cell was filled with 1M $VOSO_4$ in 2M H_2SO_4 while the right one was filled with 1M $MgSO_4$ in 2M H_2SO_4. The permeation of vanadium ion was monitored by UV/VIS spectrophotometer (760 nm) and the obtained absorbance was used to calculate the diffusion coefficient (Ks) by the equation described in literature [18]. VRFB tests were performed using a standard cell kit purchased from Standard Energy, with $9cm^2$ of effective area and 50 mL of electrolyte for each side. Graphite felt electrode was treated in air at 550 °C for 12 hours before use. 1.68 M V_2O_5 in 3 M H_2SO_4 solution with 3.5 of oxidative state of vanadium ion was purchased from Standard Energy and used as both electrolytes. Charge/discharge was performed using WBCS3000 battery cycler (WonATech) with current density ranged from $40mAcm^{-2}$ to $100mAcm^{-2}$. The coulombic efficiency (CE), voltage efficiency (VE), and energy efficiency (EE) were determined by the following equations: CE(%)=(discharge capacity/charge capacity)×100, VE(%)=(EE/CE)×100, EE(%)=(discharge energy/charge energy) ×100.

4.3. Results and Discussion

Figure 4.2(a) shows the water uptake of recast Nafion, N/GOs and N/FGOs. The water uptake values of N/GOs was similar with those of recast Nafion resulted from the hydrophilic character of GO [19], while those of N/FGOs showed decreased water uptake due to the hydrophobicity of introduced fluoroalkyl chain. The water uptake of N/GO 3 was slightly decreased due to unstable membrane formation arised from the aggregation of GO.

The volume swelling ratios of both N/GOs and N/FGOs were decreased over 10 % point compared with those of recast Nafion, indicating the enhanced dimensional stability of graphene composite membrane (Figure 4.2(b)). Although the change of swelling ratio of N/GO was differed by researches [11-13, 19], it is reasonable to explain that the interaction between Nafion matrix and GO filler has suppressed the swelling of polymer chain in this case, despite of the increased water uptake value of N/GOs. Thus the decreased swelling ratio of N/FGO can be explained with the same manner, resulted from the enhanced interaction between Nafion and FGO.

Although the water uptake values of N/FGOs were inferior to those of recast Nafion and N/GOs, the proton conductivities of N/FGOs were maintained with similar level (Figure 4.2(c)). Despite of the increased hydrophobicity of N/FGOs which significantly decreased the water uptake of N/FGOs, hydrophilic channels were successfully developed enough for protons to be transferred without hindrance, while the proton conductivities of N/GOs didn't clearly affected by the hydrophilicity of GO as reported in other researches [11, 13]. This result indirectly indicates that the hydrophobicity of FGO didn't restrain the proton conduction without accordance with the relatively low water uptake value of N/FGOs. Meanwhile the conductivity decreases roughly with increasing filler content, this was resulted from the intensified barrier effect of introduced GOs, by blocking the hydrophilic pathway.

In figure 4.2(d), vanadium ion permeability of prepared membranes are presented. Vanadium ion permeability of both N/GOs and N/FGOs were significantly decreased due to the barrier effect of GO [13]. Furthermore, N/FGO showed even lower permeability than N/GO, thus indicates the narrower hydrophilic channel formation during membrane preparation due to the hydrophobicity of fluoroalkyl chain of FGO. When the size of hydrophilic channel decreases to proper level, the permeation of vanadium ion can be inhibited while the conduction of protons not, due to larger size of vanadium ion. This explanation can be supported by the XRD analysis and SAXS analysis of previous researches about the interaction of filler material with polymer matrix and membrane casting condition affects the hydrophilic channel formation of ion exchange membranes [10, 20]. With maintained proton conductivity and decreased vanadium ion permeability, N/GOs and N/FGOs showed improved ion selectivity regardless of the filler content.

Figure 4.3 shows the VRFB performances of prepared membranes. At constant current of charge and discharge, discharge capacity decay profiles during 20 cycles of cell reaction are presented in Figure 4.3(a). Normalized capacity of recast Nafion decayed to 0.676 and one of Nafion 115 decayed to 0.725 at 19th cycle, while those of N/GOs and N/FGOs showed higher values. The capacity decaying rate of N/FGOs was slower than N/GOs roughly regardless of the filler contents, indicates the improved capacity retention of N/FGOs due to the impeded permeation of active species. Since the chemical stability, one of the main reason of capacity decay in VRFB applications, of tested membranes are maintained for over 50 cycles, it is reasonable to consider the permeation of vanadium ion is the main factor determines the capacity retention. Although N/FGO 3 showed the highest capacity retention of 0.794, the samples of N/GO 3 showed unreproducible performance due to the unstable membrane formation resulted from the aggregation of GO, N/GO 1 and N/FGO 1 was chosen for comparison for further experiments.

In Figure 4.3(b), capacity decay profiles of recast Nafion, N/GO 1, and N/FGO 1 for current density ranged from 40 to 100 $mAcm^{-2}$ are presented. At low current density, since it takes longer charging and discharging time, the permeation of vanadium ion majorly affects the cell performances, while the increase of ohmic polarization and impedance affects the cell performances at relatively higher current density. At the range of current densities experimented, the capacity retention of N/FGO 1 showed highest value among three. The decrease of the capacity with increasing current density is caused by the overpotential, which is in accordance with the experiment results.

The CE and EE of recast Nafion, N/GO 1, and N/FGO 1 are shown in Figure 4.3(c) and 4.3(d), respectively. CE of N/FGO 1 was higher than that of N/GO 1 and recast Nafion for experimented range of current densities. This result is consistent with the data of vanadium ion permeability presented in Figure 4.2(d), indicating the CE is mainly related to the permeation of active species. At high current density, the CE tends to be increased according to the short time of ion diffusion. In the same manner, the gap of CE between N/GO 1 and N/FGO 1 is decreased with increasing current density. This result is also implying that the permeation of vanadium ion is mostly impeded in N/FGOs. The EE of N/FGO 1 was higher than N/GO 1 by a small margin at 40 $mAcm^{-2}$, while it showed similar value at 60-100 $mAcm^{-2}$. Because the EE is related with the resistance of membrane, N/GO with hydrophilic character has advantages of low resistance over N/FGO with enhanced hydrophobicity. Despite of the EE at 100 $mAcm^{-2}$ of current density has an order of N/GO 1, N/FGO 1, and recast Nafion, N/FGO generally showed its advantages of VRFB cell performances for experimented range of current densities, especially at low current densities and for long-term operations.

4.4. Conclusion

Modified GO filler with hydrophobic perfluoroalkyl chain was synthesized to improve the RFB performance of Nafion membrane. Denser and narrower hydrophilic channel of N/FGO than the one of N/GO or recast Nafion lead decreased vanadium ion permeability without decrease of proton conductivity. At constant current density of 80 $mAcm^{-2}$, N/FGO showed enhanced capacity retention over 20 cycles. Coulombic and energy efficiency of N/FGO was also increased over current density ranged from 40 to 100 $mAcm^{-2}$. Increased compatibility and microstructural change of N/FGO led enhanced overall VRFB performances compared with N/GO or recast Nafion, thus make this composite membranes have the advantage for wide range of RFB applications.

4.5. References

[1] M. Ulaganathan, V. Aravindan, Q. Yan, S. Madhavi, M. Skyllas-Kazacos, T. M. Lim, Recent advancements in all-vanadium redox flow batteries, Adv. Mater. Interfaces, 3 (2016) 1500309.

[2] H. Kaneko, K. Nozaki, Y. Wada, T. Aoki, A. Negishi, M. Kamimoto, Vanadium redox reactions and carbon electrodes for vanadium redox flow battery, Electrochim. Acta, 36 (1991) 1191-1196.

[3] 2 Years Continual Running of All Vanadium Liquid Flow Storage Cell without Diminution. http://www.pemfckt.dicp.ac.cn/english/doshow1.php?id=7.

[4] C. Sun, J. Chen, H. Zhang, X. Han, Q. Luo, Investigations on transfer of water and vanadium ions across Nafion membrane in an operating vanadium redox flow battery, J. Power Sources, 195 (2010) 890-897.

[5] J. Xi, Z. Wu, X. Teng, Y. Zhao, L. Chen, X. Qiu, Self-assembled polyelectrolyte multilayer modified Nafion membrane with suppressed vanadium ion crossover for vanadium redox flow batteries, J. Mater. Chem., 18 (2008) 1232-1238.

[6] X. Teng, Y. Zhao, J. Xi, Z. Wu, X. Qiu, L. Chen, Nafion/organically modified silicate hybrids membrane for vanadium redox flow battery, J.

Power Sources, 189 (2009) 1240-1246.

[7] S. Sang, Q. Wu, K. Huang, Preparation of zirconium phosphate (ZrP)/Nafion 1135 composite membrane and $H^{+}/VO2^{+}$ transfer property investigation, J. Membr. Sci., 305 (2007) 118-124.

[8] H. J. Kim, Y.-S. Choi, M.-Y. Lim, K. H. Jung, D.-G. Kim, J.-J. Kim, H. Kang, J.-C. Lee, Reverse osmosis nanocomposite membranes containing graphene oxides coated by tannic acid with chlorine-tolerant and antimicrobial properties, J. Membr. Sci., 514 (2016) 25-34.

[9] M.-Y. Lim, Y.-S. Choi, J. Kim, K. Kim, H. Shin, J.-J. Kim, D. M. Shin, J.-C. Lee, Cross-linked graphene oxide membrane having high ion selectivity and antibacterial activity prepared using tannic acid-functionalized graphene oxide and polyethyleneimine, J. Membr. Sci., 521 (2017) 1-9.

[10] T. Ko, K. Kim, M.-Y. Lim, S. Y. Nam, T.-H. Kim, S.-K. Kim, J.-C. Lee, Sulfonated poly(arylene ether sulfone) composite membranes having poly(2,5-benzimidazole)-grapfted graphene oxide for fuel cell applications, J. Mater. Chem. A, 3 (2015) 20595-20606.

[11] L. Yu, F. Lin, L. Xu, J. Xi, A recast Nafion/graphene oxide composite membrane for advanced vanadium redox flow batteries, RSC Adv., 6 (2016) 3756-3763.

[12] K. J. Lee, Y. H. Chu, Preparation of the graphene oxide (GO)/Nafion

composite membrane for the vanadium redox flow battery (VRB) system, Vacuum, 107 (2014) 269-276.

[13] W. Dai, Y. Shen, Z. Li, L. Yu, J. Xi, X. Qiu, SPEEK/Graphene oxide nanocomposite membranes with superior cyclability for highly efficient vanadium redox flow battery, J. Mater. Chem. A, 2 (2014) 12423-12432.

[14] B. G. Kim, T. H. Han, C. G. Cho, Sulfonated graphene oxide/Nafion composite membrane for vanadium redox flow battery, J. Nanosci. Nanotechnol., 14 (2014) 9073-9077.

[15] L. Cao, Q. Sun, Y. Gao, L. Liu, H. Shi, Novel acid-base hybrid membrane based on amine-functionalized reduced graphene oxide and sulfonated polyimide for vanadium redox flow battery, Electrochinica Acta, 158 (2015) 24-34.

[16] W. S. Hummers, R. E. Offeman, Preparation of graphitic oxide, J. Am. Chem. Soc., 80 (1958) 1339-1339.

[17] Y. Zhang, S. Zhang, X. Huang, Y. Zhou, Y. Pu, H. Zhang, Synthesis and properties of branched sulfonated polyimides for membranes in vanadium redox flow battery application, Electrochim. Acta, 210 (2016) 308-320.

[18] B. Zhang, S. Zhang, D. Xing, R. Han, C. Yin, X. Jian, Quaternized poly(phthalazinone ether ketone ketone) anion exchange membrane with low permeability of vanadium ions for vanadium redox flow battery

application, J. Power Sources, 217 (2012) 296-302.

[19] B. Zhang, Y. Cao, S. Jiang, Z. Li, G. He, H. Wu, Enhanced proton conductivity of Nafion nanohybrid membrane incorporated with phosphonic acid functionalized graphene oxide at elevated temperature and low humidity, J. Membr. Sci., 518 (2016) 243-253.

[20] J. Dai, X. Teng, Y. Song, J. Ren, Effect of casting solvent and annealing temperature on recast Nafion membranes for vanadium redox flow battery, J. Membr. Sci., 522 (2017) 56-67.

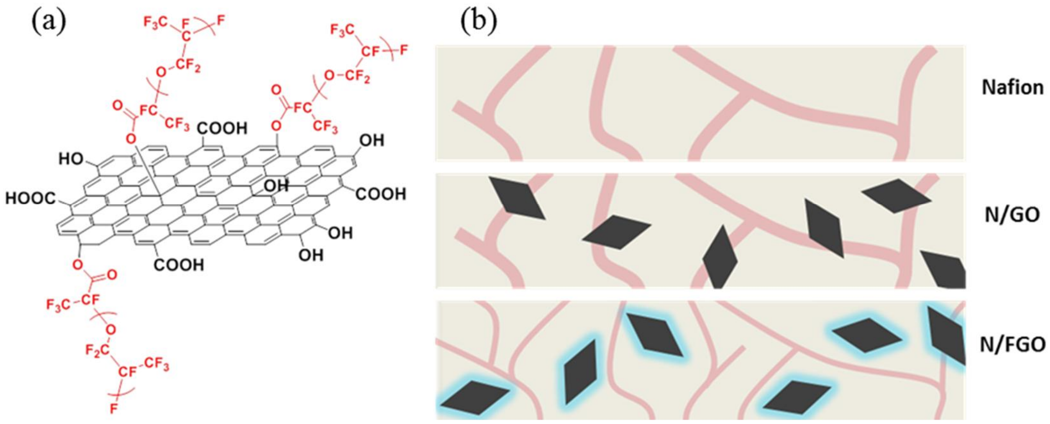

Figure 4.1. Chemical structure of FGO (a) and schematic illustration of hydrophilic channels within the membranes (b) wherein the red lines indicate the hydrophilic channels and black rectangles indicate the graphene derivatives.

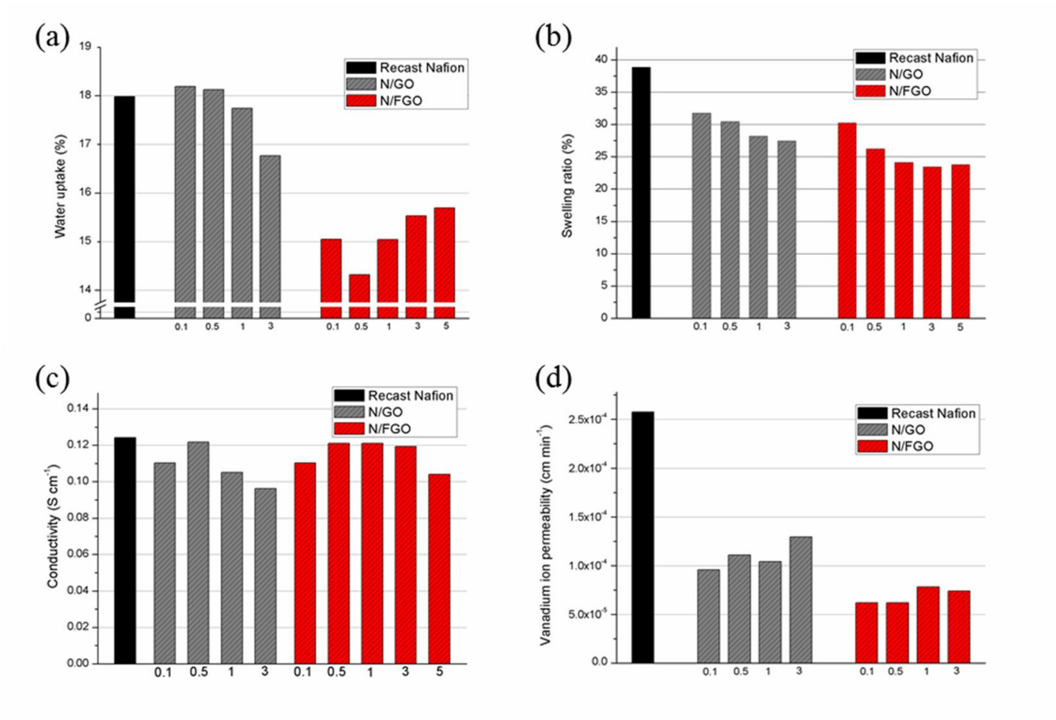

Figure 4.2. Water uptake (a), volume swelling ratio (b), proton conductivity (c), and vanadium ion permeability (d) of prepared membranes.

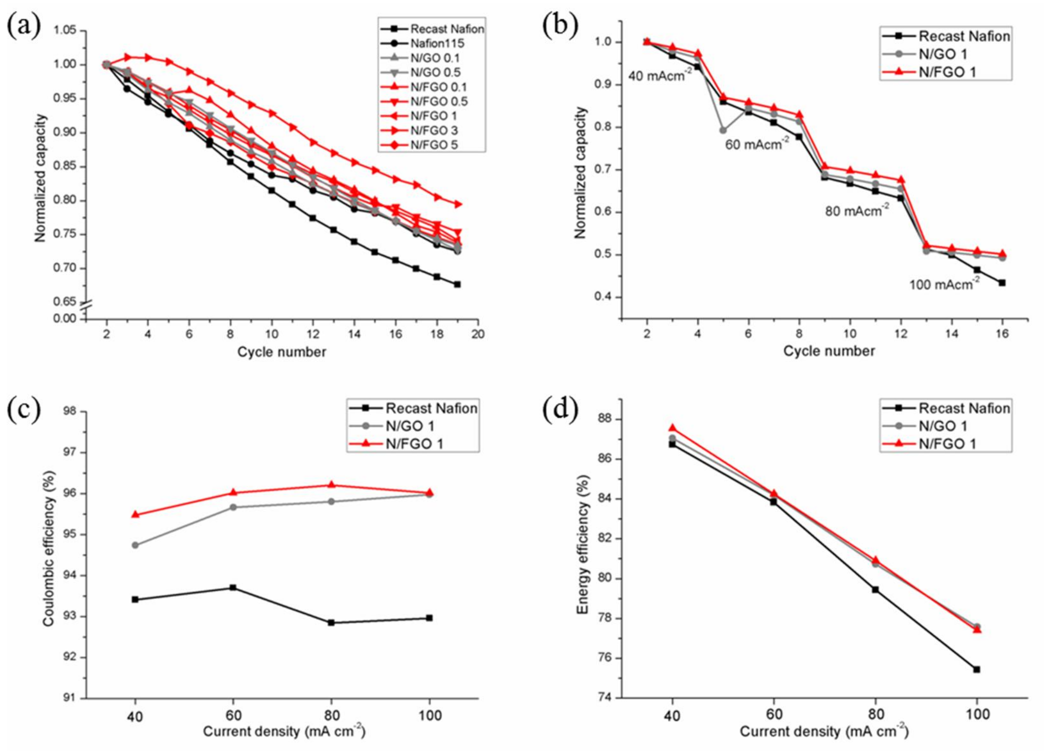

Figure 4.3. VRFB cell performances of prepared membranes, normalized discharge capacity at constant current density of 80 mAcm^{-2} (a), normalized discharge capacity (b), coulombic efficiency (c) and energy efficiency (d) at current density ranged from 40 to 100 mAcm^{-2}, respectively.

초 록

본 논문에서는 빛 또는 열에 의해 유도된 공유결합을 통해 가교가능한 자가치유 고분자와, 레독스 흐름 전지용 이온 교환막을 합성 및 분석하였다. 첫째로, 빛에 의해 가교가능한 시나메이트 작용기를 도입한 메타크릴레이트 계 고분자 (PCEMA)를 자유 라디칼 중합을 통해 합성하였다. PCEMA의 작용기가 조사하는 자외선의 파장에 따라 가역적으로 가교결합이 일어나는 것을 확인하였고 이후 유사한 구조를 갖고 유리 전이 온도가 다른 메타크릴레이트 계 고분자를 합성하여 자가치유 특성을 관찰함으로써, 유리 전이 온도 이상의 열을 가했을 때 일어나는 자가치유 특성을 확인하였다. 합성된 고분자들은 화학 반응 없이 고분자 사슬의 얽힘만으로 유리 전이 온도 이상에서 자가치유 특성을 나타내었다. 이를 통해 자가치유가 가능하며 동시에 표면 강도를 변화시킬 수 있는 자가치유 고분자를 성공적으로 합성 및 분석하였다.

둘째로, 열에 의해 가교가능한 퓨란 작용기를 도입한 메타크릴레이트 계 고분자를 자유 라디칼 중합을 통해 합성하였다. 이 고분자와 말레이미드 가교제의 딜스-알더 반응을 통해 향상된 물성을 갖는 자가치유 고분자 구조를 제조하였다. 이어 이 고분자의 자가치유 특성이 딜스-

알더 반응의 반응성에 영향을 받는 것을 확인하기 위해, 다른 전자 밀도를 갖는 퓨란 작용기를 도입한 메타크릴레이트 계 고분자를 합성하였다. 퓨란 작용기의 전자 밀도를 높임으로써 말레이미드 가교제와의 딜스-알더 반응이 촉진되었음을 확인하였고, 이에 따라 작용기의 반응성이 그에 기인한 자가치유 특성에 영향을 미치는 것을 확인하였다.

마지막으로, 레독스 흐름 전지에 쓰이는 Nafion 전해질막의 성능을 향상시키기 위하여, 그래핀옥사이드 (GO) 에 과불소화알킬 사슬을 붙인 필러 (FGO) 를 도입한 Nafion/FGO 복합체막을 제조하였다. FGO가 도입된 복합체막은 도입된 불소의 소수성으로 인한 낮은 수흡수성 및 수소이온 전도도를 보였지만, GO로 인한 향상된 치수안정성과 낮은 바나듐 이온 투과도를 보였다. 또한 필러와 Nafion의 향상된 적합성(compatibility)으로 인해 막의 결정성을 감소시키고 좁은 수소이온 채널을 형성케 함으로써 전반적인 전지 성능을 향상시키는 것을 확인하였다.

주요어: 자가치유 고분자, 가역적 공유결합, 레독스 흐름 전지, 그래핀옥사이드 유도체, 복합체막.

학번: 2011-21082 성명 : 최원재